The Transmitted Reference Pulse Cluster System for Ultra-wideband Communications

by

Li Jin

B. Eng., Shanghai Jiao Tong University, Shanghai, China, 2005

A Thesis Submitted in Partial Fulfillment of the
Requirements for the Degree of

Master of Applied Science

in the Department of Electrical and Computer Engineering

The Transmitted Reference Pulse Cluster System for Ultra-wideband Communications

by

Li Jin

B. Eng., Shanghai Jiao Tong University, Shanghai, China, 2005

Supervisory Committee

Dr. Xiaodai Dong, Supervisor (Department of Electrical and Computer Engineering)

Dr. Lin Cai, Member (Department of Electrical and Computer Engineering)

Dr. Sudhakar Ganti, Outside Member (Department of Computer Science)

Supervisory Committee

Dr. Xiaodai Dong, Supervisor (Department of Electrical and Computer Engineering)

Dr. Lin Cai, Member (Department of Electrical and Computer Engineering)

Dr. Sudhakar Ganti, Outside Member (Department of Computer Science)

Abstract

In this thesis, transmitted reference pulse cluster (TRPC) structure is proposed for low data rate ultra-wideband (UWB) communications to meet the short delay lines and low complexity requirements. TRPC contains closely and uniformly spaced pulses, and makes the analog delay lines short and easy to implement. The performance of TRPC over UWB channels is analyzed, simulated and compared to that of three existing techniques: conventional TR, non-coherent pulse position modulation (NC-PPM), and frequency shifted reference (FSR) systems. We demonstrate the performance superiority of TRPC over all those systems, especially when implementation issues such as low complexity are taken into consideration. Moreover, novel schemes are proposed to address the physical layer design issues of the TRPC structure. Based on the theoretical bit error rate (BER) derivation for TRPC, three low complexity integration interval determination schemes requiring no channel state

information are developed and simulated. In addition, an adaptive threshold method is developed for the TRPC system, which dynamically calculates the optimal detection threshold for the auto-correlation receiver, and achieves substantial performance gains over all UWB channel models.

Table of Contents

List of Figures

List of Abbreviations

Acronym	Definition
AWGN	additive white gaussian noise
BEP	bit error probability
BER	bit error rate
BPSK	binary phase shift keying
CSI	channel state information
CDMA	code division multiple access
CM	channel model
DP	dual pulse
FCC	Federal Communications Committee
FSK	frequency shift keying
GLRT	generalized likelihood ratio test
IF	intermediate frequency
i.i.d.	independent and identically distributed
IPI	inter-pulse interference
ISI	inter-symbol interference
LOS	line-of-sight
LNA	low-noise amplifier

LR-WPAN	low-rate wireless personal network
MF	matched filter
ML	maximum likelihood
NLOS	none-line-of-sight
PAR	project authorization request
PPM	pulse position modulation
PSD	power spectral density
PSK	phase shift keying
RRC	root raised cosine
RV	random variable
SNR	signal-to-noise ratio
TOA	time-of-arrival
TR	transmitted reference
UWB	ultra-wideband

Acknowledgements

First and foremost I would like to thank my supervisor, Dr. Xiaodai Dong, for her valuable guidance, continuous encouragement and insightful technical advice throughout my study. This thesis work could not have been completed without the support and help from Dr. Dong.

I would also like to thank Dr. Lin Cai, Dr. Sudhakar Ganti and Dr. Aaron Gulliver for the valuable suggestions on revising my thesis.

Thanks to many of my colleagues and friends at University of Victoria for being so nice and helpful, which makes my stay a great pleasure. Especially, I would like to thank Dr. Yue Wang, Dr. Wei Li, Dr. Zhonghua Liang, Rongrong, Ping, Fengdan, Yuzhe, Chris, Ted, Shuai, Zhuangzhuang and Shiva for their priceless help.

Special thanks to Steve, Erik, Duncan, Vicky, Moneca, Mary-Anne, Sarah and for the many patient and constant help from them.

Lastly, I would like to thank my parents, for their love, understanding, constant support, and most of all, their confidence in me and my abilities. A million words would be too short for my gratitude and I will just say, I love you, Mom and Dad.

Dedication

To my parents

Chapter 1

Introduction

1.1 Background of UWB technology

Ultra-wideband (UWB) communication, as the term suggests, is a type of communication system that transmits signal over extremely broad bandwidth. Although it did not draw vast attention until the past decade, the idea of UWB communication was already used in very first wireless transmission in human history: in Marconi Spark Gap Emitter, a UWB signal was created by the random conductance of a spark [2]. As a baseband communication utilizing a large bandwidth, the obstacles of allowing many users to efficiently share the common spectral resource caused UWB technology to remain as purely experimental work for a long time.

Since 1960s, the advances in analog and digital technology, i.e., development of the sampling oscilloscope, have made it possible for some practical UWB communication systems. Following landmark designs include the first ground-penetrating UWB-based radar in 1974 and the Micropower Impulse Radar invented in 1994. In 1999, the official name ultra-wideband was given by U. S. Department of Defense (DOD) to describe communication via transmission and reception of impulses that has band-

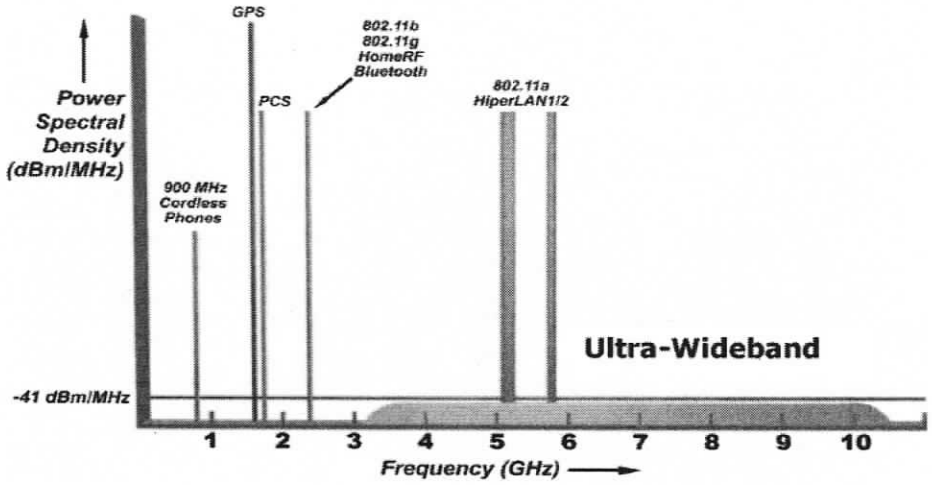

Figure 1.1: Designated UWB Spectrum from 3.1 to 10.6 GHz and Other Higher-Power Narrowband Systems [1]

width no less than 1.5 GHz or a -20 dB fractional bandwidth exceeding 25% [3]. Due to increasing demand for permission to operate unlicensed UWB systems concurrent with existing narrowband signals, in February 2002, the Federal Government Communication Committee (FCC) authorized the unlicensed use of UWB in 3.1-10.6 GHz. In contrast to the traditional regulation that FCC performed to conventional radio technology, where the spectrum is carved into narrow slices and then licensed to various users, the regulation of UWB users is to share the the broad spectrum with the existing users. To ensure that its signal will not interfere with current radio systems that the UWB system is sharing the spectrum with, UWB is operated at extremely low power levels, -41.3 dBm/Mhz, as shown in Figure 1.1, which clearly indicates that UWB signal is below the noise floor to narrowband systems.

There are two common forms of UWB: impulse UWB (I-UWB) is based on send-

ing very short duration pulses to convey information and multicarrier UWB (MC-UWB) uses multiple simultaneous carriers. This thesis is mainly focused on impulse UWB signals, which have a few features that distinguishes itself from conventional narrowband systems.

1) Baseband technology.

Since UWB has a minimum 500MHz bandwidth, by a simple $t = 1/f$ transformation, the width of a UWB transmitted waveform is in the range of a few nanoseconds or even less. Under this circumstance, the UWB signal does not need a sine-wave carrier during the transmission. Therefore, UWB is a baseband technology and will not be complicated by intermediate frequency (IF) design.

2) High time resolution.

In environments such as indoor, office and warehouse, the presence of reflectors make the multipath components extremely dense. Since UWB signals are extremely narrow, after it goes through the channel, the superposition of multiple copies of the transmitted signal will have less chance to overlap. In this case, the UWB transmitted signal is able to exploit more resolvable multipath components and thus collect the diversity. Compared to its narrowband counterpart, UWB signal suffers less fading in multipath rich environment. Meanwhile, since UWB pulses are in the range of nanoseconds, it is able to provide fine time resolution for network time distribution, as well as precise localization.

3) Low transmission power.

The FCC mask only allows UWB signal to operate on extremely low power level, which could bring constraints to UWB system design. While on the other hand, this restriction could become an advantage. Lower power level potentially means a

UWB device can last a significantly long time before the battery has to be changed, which makes it suitable to operate in rural areas where minimum support is required. In the meantime, operating at power density as low as noise makes UWB signal almost immune to possible interception. Therefore, data transmission through UWB is highly secured.

The standardization of UWB has been through several stages. It was initially designed to support High Rate Personal Area Network (HR-PAN) communication, which is regulated in the IEEE 802.15.3 Committee. To provide a higher speed UWB PHY enhancement amendment, IEEE 802.15.3a task group (TG) was formed to design a flexible standard to enable high data rate WPAN (110 Mbps at 10m, 200 Mbps at 4m and 480 Mbps at an unspecified distance) over a cost effective architecture. Since the two potential candidates – Direct Sequence (DS)-UWB supported by the UWB Forum and Multi-band Orthogonal-Frequency-Division-Multiplexing (MB-OFDM) UWB supported by the WiMedia Alliance had both strengths and weaknesses, and neither of them was able to gain the required 75 % majority needed for standards, in January 2006, the 3a group decided to withdraw the project authorization request (PAR) that was submitted in December 2002, and let the market decide which scheme will be a better fit.

Different from HR-WPAN, Low Rate WPAN (LR-PAN) is a simple, low-cost communication network that allows wireless connectivity in applications with limited power and relaxed throughput requirements. The main objectives of LR-WPAN are ease of installation, reliable data transfer, short-range operation, extremely low cost, and a reasonable battery life, while maintaining a simple and flexible protocol. Because of its ability to implement high resolution timing and precise localization at

low power level, UWB becomes a natural fit when LR-WPAN attempts to provide a PHY alternative for communications and high precision ranging/location capability. In March 2004, the IEEE 802.15 Low Rate Alternative PHY Task Group (TG4a) became an official task group. In March 2005, TG4a selected a baseline specification without enacting down-selecting procedure. The baseline consists of two optional PHYs: a UWB Impulse Radio (operating in unlicensed UWB spectrum) and a Chirp Spread Spectrum (operating in unlicensed 2.4 GHz spectrum). In March 2007, P802.15.4a was approved as a new amendment to IEEE Std 802.15.4-2006.

The UWB PHY waveform is based upon an impulse radio signaling scheme using band-limited data pulses. The UWB PHY supports three independent bands of operation: The sub-gigahertz band consists of a single channel and occupies the spectrum from 249.6 MHz to 749.6 MHz. The low band consists of four channels and occupies the spectrum from 3.1 GHz to 4.8 GHz. The high band consists of eleven channels and occupies the spectrum from 6.0 GHz to 10.6 GHz.

1.2 Transmitted Reference with UWB Communications

Since it was introduced to UWB communication in [4], transmitted reference (TR) technique has attracted substantial interest from the research and industry communities due to its simple structure and robust performance. TR does not require explicitly estimating dense multipath UWB channels and collects channel energy more easily compared to a coherent rake receiver [5]. Moreover, frequency dependent effects of a UWB channel are straightforwardly taken into account by the TR scheme. For 802.15.4a low rate applications with data rate at 1 Mbps to 2 Mbps, TR as well as energy detection schemes become right choices for receiver structures considering the

performance-cost tradeoff.

The TR technique is a subject under extensive study in the literature [4–15] (and references therein). A delay hopped TR system was first proposed in [4], and experiment results were presented in [6]. Variations to this original TR scheme were presented in [7]- [10]. Performance analysis of TR systems were carried out in [9]- [14]. In [15], a frequency multiplexed TR was proposed where the data and reference waveforms were multiplexed in disjoint frequency bands.

As mentioned before, due to the strict low power consumption requirement posed by FCC, UWB signals have to act like background noise to the existing system. Therefore, to increase the effective signal-to-noise ratio (SNR) and obtain reasonable error performance in UWB system, a data bit waveform is transmitted repeatedly over multiple "frames" in a symbol duration. The TR system follows this design, only that instead of repeating a single data pulse, the TR frame contains a pulse pair, i.e., reference (unmodulated) pulse and data (modulated) pulse. Assuming the UWB channel is slowly varying so that we may assume it remains unchanged during the period that the reference and data pulse pairs go through. Therefore, by sending the reference pulse with known polarity, the demodulation is carried out by a simple delay-and-multiply procedure, which essentially correlates the received reference and data pulses and extract the data bit. To ensure the reference and data pulse will not overlap after going through the multipath channel, the TR transmitter requires that the interval between the reference and data pulses within a frame be longer than the channel impulse response. Because the delay line in the delay-and-multiply procedure in the TR receiver must match the interval between the reference and data pulses, there is an underlining requirement that the TR receiver must be able to

implement accurate analog delay lines that are longer than the UWB channel impulse response. As of today, implementing an analog delay line longer than 10 ns is beyond the industrial capability [11] [16], while most UWB channels are longer than 20 ns. Therefore, designing a TR receiver in the real world can be very challenging.

To address the long delay line problem of TR, a frequency multiplexed TR was proposed in [15] where the data and reference waveforms were multiplexed in disjoint frequency bands. Recently, authors in [17] proposed a frequency shifted reference (FSR) scheme to avoid the use of delay lines in the traditional TR system. In [18], a dual pulse (DP) scheme that used two contiguous pulses to transmit data was proposed. The delay between the reference and data pulses is then only of pulse width T_p, which means the DP receiver only needs a T_p second delay line. The downside of this scheme is the presence of inter-pulse interference (IPI) due to closely spaced reference and data pulses and hence degraded performance compared to the conventional TR. It was proposed in [18] and [19] to mitigate IPI by analog averaging over multiple received DP frames before autocorrelation, or to completely remove IPI by using the iDP scheme. However, either solution required frame long delay lines as in the conventional TR system, except that in DP the frame length can be half the frame length in TR, i.e., $T_{f,DP} > T_m$. Therefore, the delay line problem is addressed at the price of inferior performance or frame long delay lines are required to achieve the same performance as TR. Other papers, for example, [20], analyzed the delay hopped TR scheme proposed in [4] with small T_d's. The system with IPI was modeled mathematically and efforts were focused on digital signal processing algorithm design in the receiver. The matched filter receiver, blind multiple symbol receiver and iterative receiver were proposed in [20], all of which have higher implementa-

tion complexity than the conventional TR receiver but without the long delay line requirement.

1.3 Thesis Outline

The major focus of this thesis is to propose an implementable transceiver structure that does not require channel estimation and thus suits low data rate UWB communication. A transmitted reference pulse cluster (TRPC) structure is proposed. Different from the conventional TR structure, the TRPC structure pushes the reference and data pulses close together and makes the delay line as short as the pulse width. This makes implementation of the transmitter feasible since it only requires a very short analog delay line. Although IPI is expected in the TRPC structure due to its compact nature, the evenly spaced pulse pattern and the unique detection method compensates the performance loss and even shows a substantial performance gain compared to conventional TR detection.

The thesis is organized as follows.

Chapter 2 outlines the UWB communication system that is concerned in this thesis. First a brief introduction is given on IEEE 802.15.4a channel modeling. Several modulation schemes are described which do not require channel estimation, including pulse position modulation (PPM), transmitted reference (TR), and frequency shifted reference (FSR). Demodulation method including non-coherent detection, coherent detection, square-law detection and auto-correlation detection are also depicted.

Chapter 3 proposes a new transmitted reference pulse cluster (TRPC) structure for IEEE 802.15.4a UWB communications. The performance of the TRPC versus IEEE 802.15.4a channel models is analyzed, simulated and compared with conven-

tional TR transmission, dual pulse structure, non-coherent PPM with energy detection and frequency shifted reference systems. Our results show TRPC gives the best performance among the candidates given above, especially when the implementation issues such as short analog delay lines and low complexity for UWB communications are taken into account.

Chapter 4 introduces practical data-aided algorithms to determine the integration interval for the TR pulse cluster structure. The three proposed sub-schemes have similar performance, except Scheme C suffers some degradation in IEEE 802.15.4a channel model 1 environments. For implementation, Scheme A requires either high sampling rate for digital processing or analog averaging with symbol long delay lines, and Scheme C involves multiple two dimensional search procedures. In comparison to A and C, Scheme B is the best candidate in terms of performance and implementation complexity.

Chapter 5 proposes an adaptive threshold scheme for the TR pulse cluster system which modifies the decision threshold for each particular channel realization to ensure (close to) identical conditional BERs and hence leads to improved average performance. Simulation results show that this scheme achieves performance gains from 0.5 dB to 2.0 dB for the TR pulse cluster system in IEEE 802.15.4a channel models.

Chapter 6 concludes the thesis and proposes the future work.

Chapter 2

UWB Communication Systems

2.1 IEEE 802.15.4a Channel Model

In wireless communication system, the received signal is an attenuated, delayed, and possibly distorted version of the transmitted signal plus noise and (possibly) interference. The relationship between the received signal and the transmitted signal is typically called the "channel". The generic 802.15.4a channel model [21] adopts the Saleh-Valenzuela [22] shape and is used for 100-1000 MHz and 2-10 GHz model. [1] It is the physical realization that multipath components arrive in clusters and has its impulse response represented by

$$h_{discr}(t) = \sum_{l=0}^{L} \sum_{k=0}^{K} a_{k,l} \exp(j\phi_{k,l}) \delta(t - T_l - \tau_{k,l}) \tag{2.1}$$

where $a_{k,l}$ and $\phi_{k,l}$ are the tap weight and the phase of the k-th ray in the l-th cluster, with $\phi_{k,l}$ uniformly distributed over the range $[0, 2\pi]$, L is the number of the clusters

[1] The 1 MHz channel model and the body-area network channel model are different from this generic channel model, which are out of the scope of this thesis.

which follows Poisson-distribution as

$$pdf_L(L) = \frac{(\bar{L})^L \exp(-\bar{L})}{L!}. \tag{2.2}$$

The cluster arrivals are described as a Poisson process with mean arrival rate Λ; within each cluster, the component arrivals are also described as a Poisson process with parameter λ, where $\lambda \gg \Lambda$. The arrival time of the l-th cluster is denoted by T_l, and the arrival time of the k-th component within the l-th cluster is denoted by $\tau_{k,l}$. Then according to the model, there is

$$p(T_l|T_{l-1}) = \Lambda \exp[-\Lambda(T_l - T_{l-1})], \quad l > 0, \tag{2.3}$$

$$p(\tau_{k,l}|\tau_{k-1,l}) = \lambda \exp[-\lambda(\tau_{k,l} - \tau_{k-1,l})], \quad k > 0. \tag{2.4}$$

Due to the discrepancy in the fitting for the different indoor and outdoor scenarios, the arrival time of multipath component given by (2.4) is updated with a mixture of two Poisson processes [21]

$$p(\tau_{k,l}|\tau_{k-l,l}) = \beta\lambda_1 \exp[-\lambda_1(\tau_{k,l} - \tau_{k-1,l})] + (1-\beta)\lambda_2 \exp[-\lambda_2(\tau_{k,l} - \tau_{k-1,l})], \quad k > 0 \tag{2.5}$$

where β is the mixture probability, while λ_1 and λ_2 are the ray arrival rates.

The cluster energy decays exponentially such that the average power of the l-th cluster Ω_l is given by

$$10\log(\Omega_l) = 10\log(\exp(-T_l/\Gamma)) + M_{cluster} \tag{2.6}$$

where Γ is the cluster exponential decay factor and $M_{cluster}$ is a normally distributed variable with standard deviation $\sigma_{cluster}$ around it.

Similar to the inter-cluster situation, the mean power of the k-th multipath component within the l-th cluster also decays exponentially and can be presented by

$$\Omega_{k,l} = \frac{\Omega_l}{\gamma_l[(1-\beta)\lambda_1 + \beta\lambda_2 + 1]} \exp(-\tau_{k,l}/\gamma_l) \tag{2.7}$$

where Ω_l is the integrated energy of the l-th cluster given by (2.6), and γ_l is the component exponential decay factor.

For non-line-of-sight (NLOS) case of some environments (office and industrial) where the reflection of the signal might result in larger received energy, the shape of the power delay profile does not follow the exponential decay as in (2.7). Instead, it has a distribution with a rising period followed by decay as in

$$\Omega_{k,l} = (1 - \chi \cdot \exp(-\tau_{k,l}/\gamma_{rise})) \cdot (-\tau_{k,l}/\gamma_1) \cdot \frac{\gamma_1 + \gamma_{rise}}{\gamma_1} \frac{\Omega_l}{\gamma_1 + \gamma_{rise}(1-\chi)} \tag{2.8}$$

where parameter χ describes the attenuation of the first ray, the parameter γ_{rise} determines how fast the power delay profile increases to its local maximum, and γ_1 determines the decay at late times.

After the power delay profile is derived, the small scale fading is modeled as Nakagami so that the weight of the tapped delay $a_{k,l}$ follows the distribution

$$p_{a_{k,l}}(a) = \frac{2}{\Gamma(m)} (\frac{m}{\Omega_{k,l}})^m a^{2m-1} \exp(-\frac{m}{\Omega_{k,l}} a^2) \tag{2.9}$$

where the m-parameter is modeled as a lognormally distributed random variable with

logarithm mean μ_m and standard deviation σ_m, and $\Omega_{k,l}$ is given by (2.7) or (2.8), depending on the specific scenarios.

The above specification lays out the channel model.[2] In the prototype code provided within [21], 9 different scenarios are modeled with complete set of parameters. Although suitable for simulation, the generic model is very complicated for analytical derivation. Therefore, all the analysis done to the UWB channels are based on the tapped delay model, which generalizes the channel as a simple tapped delay lines as

$$h(t) = \sum_{k=0}^{K-1} \alpha_k \delta(t - \tau_k) \tag{2.10}$$

where α_k and τ_k are the complex amplitude and delay of the k-th component.

2.2 LR-WPAN Modulation and Detection Schemes

As described in Section 2.1, the IEEE 802.15.4a channels consist of numerous multipath components and thus the channel estimation becomes extremely challenging. Therefore, various schemes were brought up which are able to demodulate the received signal without knowledge of the channel. Among them, three schemes are considered in this thesis: transmitted reference (TR), frequency shifted reference (FSR) modulation and non-coherent pulse position modulation (NC-PPM).

2.2.1 Transmitted Reference Modulation

The transmitted reference (TR) system was first proposed in 1920s. In a TR system, a pair of unmodulated and modulated pulses are transmitted through a slowly varying

[2]The antenna effect is not included since for wideband systems the antenna effects is no longer negligible and should be taken care of in a separate matter; also the large-scale fading is not discussed here.

channel, and the former is employed to demodulate the latter. The two pulses, which are named as reference and data pulses, respectively, are separated by a certain delay T_d. The polarity of the reference pulse is known to the receiver (always chosen to be "1" for convenience) and the polarity of the data pulse is modulated by the binary bit that is transmitted over the channel. In a system adopting binary phase shifted keying (BPSK), the bit "1" is represented by a data pulse with the same polarity as the reference pulse, and the bit "0" is represented by a data pulse that is antipodal to the reference pulse. In other words, the transmitted bit is encoded as the polarity difference between the reference pulse and data pulse. In LR-UWB systems, these pulse pairs are repeated over many frames to increase the aggregation at the receiver. The mathematical representation of the TR structure is

$$s_{TR}^{(m)}(t) = \sqrt{E_p} \sum_{n=0}^{N_f-1} \left[p(t - nT_f) + b_m p(t - nT_f - T_d) \right]. \tag{2.11}$$

The transmitted signal consists of N_f pulse pairs with pulse energy E_p and pulse width T_p, T_f is the pulse repetition period, and $b_m \in \{1, -1\}$ is the m-th bipolar information bit. In order to avoid inter-pulse interference, the delay between the pulse pair T_d is designed to be longer than channel delay spread, i.e., $T_d > \tau_{K-1}$. Meanwhile, to prevent the data pulse interfering the reference pulse of the next frame, there has $T_d + \tau_{K-1} < T_f$. An example of TR transmission pattern is shown in Fig. 2.1, with the pulse repetition number $N_f = 2$, and the transmitted bits are $\{1, -1, -1\}$.

After the TR signal goes through the multipath channel as in (2.10), the received

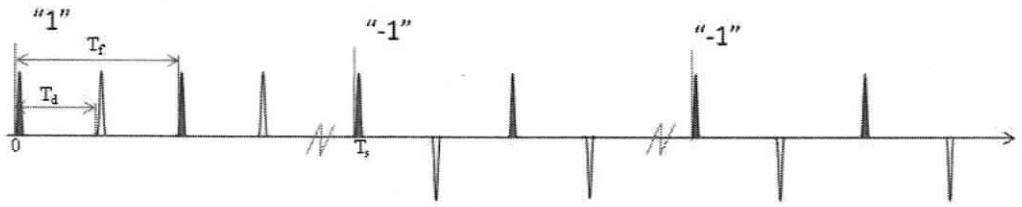

Figure 2.1: Pulse pattern of transmitted reference (TR) communication with $N_f = 2$, transmitted bits $=\{1, -1, -1\}$; shadowed pulses represent reference pulses and unshadowed pulses represent data pulses

signal can be written as

$$r_{TR}^{(m)}(t) = \sqrt{E_p} \sum_{k=0}^{K-1} \sum_{n=0}^{N_f-1} \alpha_k \left[p(t - nT_f - \tau_k) + b_m p(t - nT_f - T_d - \tau_k) \right]. \qquad (2.12)$$

The biggest advantage of the TR signalling is that the demodulation is carried out by correlating the modulated signal part with the unmodulated signal part. Since the the pair of the pulses go through the same channel (assuming a slow fading channel is used), the polarity of the correlation indicates the polarity of the transmitted bit. The mathematical expression of the demodulation is

$$D_{TR}(m) = \mathrm{R} \left\{ \sum_{n=0}^{N_f-1} \int_0^T r_{TR}^{(m)}(t + nT_f) r_{TR}^{*(m)}(t + nT_f + T_d) dt \right\} \qquad (2.13)$$

and the detection is carried out by $D_{TR}(m) \underset{b_m=\text{“0”}}{\overset{b_m=\text{“1”}}{\gtrless}} 0$.

2.2.2 Frequency Shifted Reference

Also designed to tackle the analog delay element difficulty, a slightly frequency-shifted reference (FSR) technique was proposed in [17] for LR-UWB applications. It keeps the reference-data format as in standard TR-UWB, but replaces the time delay element with a frequency translation. In other words, the data pulse is translated in frequency (rather than in time) to be orthogonal to the reference signal. The transmitted FSR signal over interval $[mT_s, (m+1)T_s]$ is given by

$$s_{FSR}(t) = \sqrt{\frac{E_s}{2}} u(t - mT_s) + \sqrt{E_s} b_m u(t - mT_s) \cos(2\pi f_0 t) \tag{2.14}$$

where E_s is the energy per symbol. The reference pulse in FSR is unmodulated while the data pulse is modulated by b_m and frequency shifted by $\cos(2\pi f_0 t)$. After the FSR signal passes through the multipath channel $h(t) = \sum_{k=0}^{K-1} \alpha_k \delta(t - \tau_k)$, the received signal is thus written as

$$r(t) = \sum_{k=0}^{K-1} \alpha_k x(t - \tau_k). \tag{2.15}$$

The detection is carried out by "correlating" the reference and data signals. Since reference and data pulses are essentially staying on the same time slot, the delay-and-multiply action becomes square. The mathematical expression is

$$D_{FSR}(m) = \int_0^{T_s} r^2(t) \sqrt{2} \cos(2\pi f_0 t) dt \tag{2.16}$$

and the decision is made by $D_{FSR}(m) \underset{b_m=\text{“0”}}{\overset{b_m=\text{“1”}}{\gtrless}} 0$.

2.2.3 Non-coherent Pulse Position Modulation

The IEEE 802.15.4a standard [23] adopts non-coherent pulse position (NC-PPM) modulation with energy detection. The PPM signal $s_{NC-PPM}(t)$ specified in the IEEE 802.15.4a standard consists of 8 pulses with short, uniform spacing instead of a single pulse for one information bit to meet FCC mask. During the m-th bit interval $t \in [(m-1)T_s, mT_s]$, the transmitted signal (including the receiver matched filter) is given by

$$s_{NC-PPM}(t) = (1 - b_m)\sqrt{\frac{E_b}{2N_f}}s(t) + b_m\sqrt{\frac{E_b}{2N_f}}s(t - \frac{T_s}{2}) \tag{2.17}$$

where the information bit $b_m \in \{-1, 1\}$ decides which part of the symbol interval that $s(t)$ sits in. Since $s(t)$ in [19] has similar structure to TRPC, we can use either the "+1" pulse cluster $s(t) = s_{+1}(t)$ or the "-1" pulse cluster $s(t) = s_{-1}(t)$ for transmission, as shown in Fig. 2.2. As the "+1" pulse cluster is not the antipolar version of the "-1" pulse cluster, it is expected that the PPM structures adopting "+1" and "-1" pulse cluster would give different BER performance. The received signal after going through the UWB channel and AWGN is then given by

$$r(t) = \sum_{k=0}^{K-1} \alpha_k \tilde{s}(t - \tau_k) + n(t) = \sqrt{\frac{E_b}{2N_f}}v(t) + n(t) \tag{2.18}$$

where $v(t) = \sqrt{\frac{2N_f}{E_b}}\sum_{k=0}^{K-1} \alpha_k \tilde{s}(t - \tau_k)$. The receiver employs two simple energy detectors to demodulate the received signal. The outputs of the two energy detectors are given by

$$V_0 = \int_{t_b}^{t_e} |r(t)|^2 dt \tag{2.19}$$

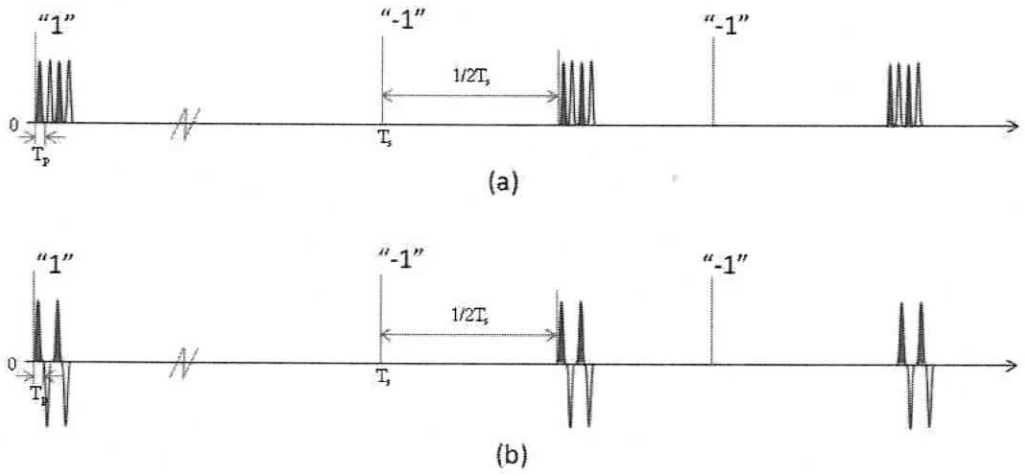

Figure 2.2: Pulse pattern of non-coherent pulse position modulation (NC-PPM) with $N_f = 2$, transmitted bits $=\{1, -1, -1\}$; figure (a) uses "+1" cluster and figure (b) uses "-1" cluster.

and

$$V_1 = \int_{t_b+\frac{T_s}{2}}^{t_e+\frac{T_s}{2}} |r(t)|^2 dt. \tag{2.20}$$

If $V_0 > V_1$, a decision on "0" is made; otherwise, a decision on "1" will be made. The integration interval is determined using the method similar to the TR pulse cluster system, where $t_b = T_l$ and $t_e = T_h + 2(N_f - 1)T_d$ with the interval $[T_l, T_h]$ containing sufficient energy of the channel.

Suppose "0" is transmitted, the energy detector output V_0 can be further written as

$$V_0 = D_1 + D_2 + D_3 + D_4 \tag{2.21}$$

where

$$\begin{aligned} D_1 &= \frac{E_b}{2N_f} \int_{T_1}^{T_2} |v(t)|^2 dt \\ D_2 &= \sqrt{\frac{E_b}{2N_f}} \int_{T_1}^{T_2} v(t) n^*(t) dt \\ D_3 &= \sqrt{\frac{E_b}{2N_f}} \int_{T_1}^{T_2} v^*(t) n(t) dt \\ D_4 &= \int_{T_1}^{T_2} |n(t)|^2 dt. \end{aligned} \tag{2.22}$$

The energy detector output V_1 is given by

$$V_1 = \int_{T_1+\frac{T_s}{2}}^{T_2+\frac{T_s}{2}} |n(t)|^2 dt. \tag{2.23}$$

The final decision variable is then given by

$$D = V_0 - V_1 = D_1 + D_2 + D_3 + D_4 - V_1. \tag{2.24}$$

Again, D can be approximated as a Gaussian RV with mean D_1. Because D_2, D_3, D_4 and V_1 are independent, the variance of D is given by

$$\sigma_D^2 = \frac{E_b N_0}{N_f} \int_{T_1}^{T_2} \int_{T_1}^{T_2} \mathrm{Re}\{v(t)v^*(t')\} R_{tr}(t'-t)dtdt' + 2N_0^2 \int_{-\frac{T_i}{\sqrt{2}}}^{\frac{T_i}{\sqrt{2}}} (\sqrt{2}T_i - 2|y|) R_{tr}^2(\sqrt{2}y)dy. \tag{2.25}$$

Therefore, the conditional probability of error for the non-coherent detection of binary PPM is expressed as

$$P(e|\mathbf{h}) = P(D < 0) = Q\left(\frac{D_1}{\sigma_D}\right). \tag{2.26}$$

Chapter 3

Transmitted Reference Pulse Cluster System in Ultra-wideband Communications

3.1 TRPC System Model and Performance Analysis

To utilize the reference pulses for demodulation and also address the analogy delay line implementation issue in UWB communication, the transmitted reference pulse cluster (TRPC) system is developed.

The pulse structure of a TRPC system is shown in Fig. 3.1. A dual pulse pair composed of a reference pulse and a data pulse with short delay T_d is repeated uniformly every $2T_d$ seconds. Mathematically, the TRPC signal (including the receiver

matched filter) can be represented by

$$\begin{aligned}\hat{s}(t) &= \sqrt{\frac{E_b}{2N_f}} \sum_{m=-\infty}^{\infty} \sum_{i=0}^{N_f-1} [g(t - mT_s - 2iT_d) + b_m g(t - mT_s - (2i+1)T_d)] \\ &= \sqrt{\frac{E_b}{2N_f}} \sum_{m=-\infty}^{\infty} s_{b_m}(t - mT_s) \end{aligned} \tag{3.1}$$

where E_b is the average energy per bit, N_f is the number of repeated dual pulse pairs in one cluster, $g(t)$ is the composite pulse with duration T_p resulting from the convolution of the transmitter pulse $g_{tr}(t)$ and the receiver filter matched to $g_{tr}(t)$, T_s is the symbol duration determined by the bit rate, $b_m \in \{+1, -1\}$ is the m-th bipolar information bit, and $s_{b_m}(t) = \sum_{i=0}^{N_f-1} g(t - 2iT_d) + b_m \sum_{i=0}^{N_f-1} g(t - (2i+1)T_d)$. The delay T_d between the reference pulse and data pulse can be set as short as T_p, or $T_p \leq T_d < 10$ ns. In Fig.3.1(a), T_d is equal to pulse width T_p, and in Fig.3.1(b), $T_d = 2T_p$. The TR pulse cluster bearing data "+1" is called the "+1" pulse cluster and the other "-1" pulse cluster, as given by

$$\begin{aligned} s_{+1}(t) &= \sum_{i=0}^{N_f-1} g(t - 2iT_d) + g(t - (2i+1)T_d) \\ s_{-1}(t) &= \sum_{i=0}^{N_f-1} g(t - 2iT_d) - g(t - (2i+1)T_d). \end{aligned} \tag{3.2}$$

Since $s_{+1}(t) \neq -s_{-1}(t)$, the difference between the "+1" and "-1" pulse clusters is not simply a (-1) factor. This is in contrast to the conventional binary phase shift keying (BPSK) modulation.

Unlike the conventional TR that looses 3 dB in signal power due to the transmission of the non-information bearing reference pulse, the reference pulses in TRPC can

be used with the data pulses in the previous pairs to collect energy for data detection, in addition to the energy collected as in the conventional TR. This is illustrated in Fig. 3.2. In this figure, a "-1" pulse cluster is transmitted, where $N_f = 4$. The solid pulses denote the reference pulses and the dashed pulses denote the data pulses. The energy of each pulse is $E_b/2N_f$. At the receiver, the received signal is correlated with its T_d delayed copy. Assuming an additive white Gaussian noise (AWGN) channel, the overall energy collected for data detection in TRPC is given by

$$E_{\text{TRPC}} = (2N_f - 1) \cdot \frac{E_b}{2N_f} \approx E_b. \tag{3.3}$$

Whereas in the conventional TR system, energy is only collected for the correlation between the data pulses and reference pulses within the pairs, as illustrated by the four blank rectangles in Fig. 3.2. That is,

$$E_{\text{conventionalTR}} = N_f \cdot \frac{E_b}{2N_f} = \frac{1}{2}E_b. \tag{3.4}$$

Theoretically, the energy collected in TRPC could be arbitrarily close to E_b by increasing N_f. In implementation, N_f can not be too large because in this case, the energy per pulse would be too low to combat the noise effect. In other words, a large N_f would lead to a longer pulse cluster and also a longer integration interval, which would introduce more noise to the autocorrelation receiver and impair the performance. As a result, N_f is a parameter that can be optimized in the TR pulse cluster structure. Apparently, the uniform spacing among all reference and data pulses in the cluster is crucial to the performance of TRPC and the cluster is treated as a

whole entity in the detection. This is fundamentally different from the delay hopped TR in the literature.

In realistic UWB channels, the interference among the reference and data pulses caused by multipath will be present. The UWB channel described by IEEE 802.15.4a channel models can be generalized as [21]

$$h(t) = \sum_{k=0}^{K-1} \alpha_k \delta(t - \tau_k) \tag{3.5}$$

where α_k and τ_k are the complex amplitude and delay of the k-th multipath. The received signal after the lowpass matched filter $g_{tr}(t)$ can then be written as

$$\begin{aligned} r(t) &= \sum_{k=0}^{K-1} \alpha_k \tilde{s}(t - \tau_k) + n(t) = \sqrt{\frac{E_b}{2N_f}} \sum_{k=0}^{K-1} \alpha_k \sum_{m=-\infty}^{\infty} s_{b_m}(t - \tau_k - mT_s) + n(t) \\ &= \sqrt{\frac{E_b}{2N_f}} \sum_{m=-\infty}^{\infty} q_m(t - mT_s) + n(t) \end{aligned} \tag{3.6}$$

where $q_m(t) = \sum_{k=0}^{K-1} \alpha_k s_{b_m}(t - \tau_k)$, and $n(t)$ is the complex additive white Gaussian noise filtered by $g_{tr}(t)$. The autocorrelation function of $n(t)$ is given by $R_n(\tau) = E[n^*(t)n(t+\tau)] = N_0 R_{tr}(\tau)$, where $R_{tr}(\tau) = \int_{-\infty}^{\infty} g_{tr}(t) g_{tr}(t+\tau) dt$ and N_0 is the power spectral density of the complex white Gaussian noise.

The receiver performs auto-correlation on the received signal and its T_d delayed version. The decision variable (DV) for the m-th bit is given by

$$D = \int_{mT_s + t_b}^{mT_s + t_e} r(t) r^*(t - T_d) dt. \tag{3.7}$$

The receiver makes a decision on "1" if $\mathrm{Re}\{D\} > 0$, and "0" if $\mathrm{Re}\{D\} < 0$. The choice

of the integration interval $[t_b, t_e]$ is critical to the success of the detection scheme. In order to ensure that we capture all the energy in the received pulse cluster, we select the integration interval as follows: $t_b = T_d + T_l$, $t_e = T_d + 2(N_f - 1)T_d + T_h + T_p = (2N_f - 1)T_d + T_h + T_p$, where T_l and T_h are the beginning and end time of the UWB channel for integration, respectively. Usually T_l is close to be the time-of-arrival (TOA) of the first significant path of the channel, especially in a line-of-sight (LOS) environment, and the interval $[T_l, T_h]$ should include sufficient channel energy for detection. Such choices of t_b and t_e guarantee that the auto-correlation covers the significant channel portion plus a duration of $2(N_f - 1)T_d + T_p$ related to the pulse cluster width. It is obvious from (3.7) that the receiver is very simple and only needs a T_d long delay line.

Some discussions on TRPC are presented here.

Remark 1 (Noise reduction due to short integration interval): Note that in TRPC, the integration length of the autocorrelation detector is around the cluster width plus the length of the channel that has significant multipaths. In the conventional TR, integration performed in each frame is over the pulse width plus the length of the channel that has significant multipaths, and it is done with N_f frames. The effective integration length of conventional TR is much longer than that of TRPC. The shorter integration interval makes the noise component included in the TRPC detection much smaller, leading to substantial performance improvement over the conventional TR, especially when the system signal-to-noise ratio is not very high.

Remark 2 (Simple detector with noise averaging): In the conventional TR systems, noise averaging can be carried out in two ways. The received signal can be first added frame over frame for analog noise averaging and then followed by autocorrelation. Al-

ternatively, autocorrelation is first performed in each frame and the results are added to reduce noise in the decision variable. The former has better performance, but requires frame long delay lines. In the proposed receiver for TRPC, the second type of noise averaging is implicitly performed in the operation. The detector delays the received cluster by T_d and then performs correlation on the whole cluster. The summation procedure for noise averaging is automatically included by the integrator in TRPC. Moreover, additional energy for data detection is collected in the correlation due to the uniform structure of TRPC, as demonstrated in (3.3) and (3.4).

Remark 3 (ISI free and possible multiple-access): In the TRPC system, since T_d is much shorter than 10 ns and the repetition within one symbol is $N_f = 4$, we have the pulse cluster width $T_u = 2N_f T_d < 80$ ns. For $T_d = 2.02$ ns, $T_u = 16.16$ ns. Given low data rate transmission such as 1Mbps in 802.15.4a channels, the pulse cluster only occupies a small portion of the symbol duration, which is indicated as S in Fig. 3.1. It is known that the average delay of 802.15.4a channels is in the range of [50, 200] ns. Therefore after the pulse cluster is passed through the multipath channel, the resulting signal is still shorter than the symbol duration. By "squeezing" the signal within a small portion of the symbol duration, the occurrence of ISI is minimized. This is in contrast to the conventional TR where pulses are spread over the whole symbol duration in the form of multiple frames.

Moreover, considering a multiple access scenario, we can divide a symbol duration into multiple time slots as shown in Fig. 3.1, and each user occupies a different time slot where a TR pulse cluster resides. If time hopping is desired, it can be performed on TR pulse clusters from time slot to time slot instead of hopping within each cluster. Similarly, scrambling, if to be used, should be carried out on a pulse cluster

basis as well.

Next we derive the bit error rate (BER) of TRPC conditional on a given UWB channel. The subsequent analysis on (3.7) involves only one symbol, hence the subscript m is omitted for convenience. Assuming the symbol interval T_s is sufficiently long so that there is no inter-symbol interference (ISI), we have

$$\begin{aligned}
D &= D_1 + D_2 + D_3 + D_4 \\
D_1 &= \frac{E_b}{2N_f}\int_{t_b}^{t_e}\sum_{l=0}^{K-1}\sum_{k=0}^{K-1}\alpha_l\alpha_k^* s(t-\tau_l)s^*(t-\tau_k-T_d)dt = \frac{E_b}{2N_f}\int_{t_b}^{t_e} q(t)q^*(t-T_d)dt \\
D_2 &= \sqrt{\frac{E_b}{2N_f}}\int_{t_b}^{t_e} q(t)n^*(t-T_d)dt \\
D_3 &= \sqrt{\frac{E_b}{2N_f}}\int_{t_b}^{t_e} q^*(t-T_d)n(t)dt \\
D_4 &= \int_{t_b}^{t_e} n(t)n^*(t-T_d)dt
\end{aligned} \tag{3.8}$$

where D_1 is the signal-signal component, D_2 and D_3 are the random variables (RVs) representing the signal-and-noise product, and D_4 is an RV accounting for the noise-noise product. It can be easily shown that $E[D_2+D_3]=0$ and $E[D_4]\approx 0$ as $T_d \geq T_p$. Therefore, the mean of $\mathrm{Re}\{D\}$ is given by (3.9),

$$\begin{aligned}
m_D(b_m) &= E[\mathrm{Re}\{D\}] \approx \mathrm{Re}\{D_1\} = \frac{E_b}{2N_f}\int_{t_b}^{t_e}\mathrm{Re}\{q(t)q^*(t-T_d)\}dt \\
&= \frac{E_b}{2N_f}[(2N_f-1)E_gE_hb_m + \sum_{l=K_1}^{K_2}\sum_{\substack{k=K_1 \\ k\neq l}}^{K_2}\mathrm{Re}\{\alpha_l\alpha_k^*\}R_{ss}(|T_d-\tau_l+\tau_k|)]
\end{aligned} \tag{3.9}$$

where E_g is the energy in the pulse $g(t)$, $E_h = \sum_{k=K_1}^{K_2} |\alpha_k|^2$ is the channel energy collected by the integration interval $[t_b, t_e]$, and $R_{ss}(\tau) = \int_{-\infty}^{\infty} s(t)s(t+\tau)dt$. The first term is the TRPC energy collected from multipaths for data detection, and the second term represents the IPI. Analysis for D_2, D_3 and D_4 is similar to [19], [11]. These RVs can be closely approximated as Gaussian distributed, especially now that a pulse cluster is longer than a single dual pulse. To calculate the bit error rate of TRPC, we need to know the variance of the Gaussian RV $\mathrm{Re}\{D\}$. It can be easily shown that Gaussian RVs $D_2 + D_3$ and D_4 are independent, therefore the variance of $\mathrm{Re}\{D\}$ is the sum of $\sigma_{23}^2(b_m) = \mathrm{Var}[\mathrm{Re}\{D_2 + D_3\}]$ and σ_4^2. In particular,

$$\sigma_4^2 = \mathrm{Var}[\mathrm{Re}\{D_4\}] = \frac{N_0^2}{2} \int_{-\frac{T_i}{\sqrt{2}}}^{\frac{T_i}{\sqrt{2}}} (\sqrt{2}T_i - 2|y|) R_{tr}^2(\sqrt{2}y)dy \tag{3.10}$$

where $T_i = t_e - t_b$, and $\sigma_{23}^2(b_m)$ is given by

$$\begin{aligned}
\sigma_{23}^2(b_m) &= \mathrm{Var}[\mathrm{Re}\{D_2\}] + \mathrm{Var}[\mathrm{Re}\{D_3\}] + 2\mathrm{E}[\mathrm{Re}\{D_2\}\mathrm{Re}\{D_3\}] \\
\mathrm{Var}[\mathrm{Re}\{D_2\}] &= \frac{E_b N_0}{4N_f} \int_{t_b}^{t_e} \int_{t_b}^{t_e} \mathrm{Re}\{q(t)q^*(t')\} R_{tr}(t'-t)dtdt' \\
\mathrm{Var}[\mathrm{Re}\{D_3\}] &= \frac{E_b N_0}{4N_f} \int_{t_b}^{t_e} \int_{t_b}^{t_e} \mathrm{Re}\{q(t-T_d)q^*(t'-T_d)\} R_{tr}(t'-t)dtdt' \\
E[\mathrm{Re}\{D_2\}\mathrm{Re}\{D_3\}] &= \frac{E_b N_0}{4N_f} \int_{t_b}^{t_e} \int_{t_b}^{t_e} \mathrm{Re}\{q(t)q^*(t'-T_d)\} R_{tr}(t'-t+T_d)dtdt'.
\end{aligned} \tag{3.11}$$

As mentioned before, because the difference between the "+1" and "-1" pulse cluster is not the simple (-1) factor, the error probability of "+1" pulse cluster is not necessarily identical to that of the "-1" pulse cluster. Therefore, the probability of

error for the TR scheme conditioned on the channel realization $\mathbf{h}$ is given by

$$\begin{aligned} P(e|\mathbf{h}) &= P(e|\mathbf{h}, b_m = 1)P(b_m = 1) + P(e|\mathbf{h}, b_m = -1)P(b_m = -1) \\ &= \frac{1}{2}Q\left(\frac{-m_D(-1)}{\sqrt{\sigma_{23}^2(-1) + \sigma_4^2}}\right) + \frac{1}{2}Q\left(\frac{m_D(1)}{\sqrt{\sigma_{23}^2(1) + \sigma_4^2}}\right) \end{aligned} \tag{3.12}$$

where $\mathbf{h} = \{(\alpha_k, \tau_k)|k = 0, ..., K-1\}$.

3.2 Simulation and Numerical Results

In this section, we present simulation and numerical results of the proposed TRPC system. To show the superiority of the TRPC system, we also give the simulation results of several alternative schemes – non-coherent pulse position modulation, the conventional TR system and frequency shift reference system. Two representative channels are chosen for simulation, i.e., IEEE 802.15.4a CM1 and CM8 channels. CM1 models strong line-of-sight (LOS) channels and CM8 models Non-LOS (NLOS) channels with an extremely large delay spread [21]. The non-coherent PPM system employs either *all* "+1" or *all* "-1" pulse cluster placed at different time slots within a symbol and the position of the pulse cluster represents information data. The conventional TR system spreads out N_f reference and data pulse pairs evenly in one symbol duration. The frequency shift reference translates the reference pulse in the frequency domain. We did not include time hopping in the conventional TR since it does not affect single user conventional TR performance assuming IPI and inter-frame interference (IFI) free. Here is a description of the system parameters. The transmitter pulse shape filter and the receiver filter are the root raised cosine (RRC) pulse with roll-off factor $\beta = 0.25$. The zero-to-zero main lobe width of the

RRC pulse is $T_p = 2.02$ ns, and a truncated RRC pulse of duration $8T_p$ is used in the simulation. The pulse cluster is composed of 8 contiguous pulses, i.e., $N_f = 4$. The pulse cluster length is then $T_u = 16.16$ ns. Low bit rates of 2 Mbps for CM1 and 1 Mbps for CM8 are studied, and hence the system is ISI free. The sampling rate of the receiver analog-to-digital (A/D) device is equal to the symbol rate, i.e., 2 MHz and 1 MHz for CM1 and CM8 channels respectively. The integration interval related parameters T_l and T_h are determined as the beginning and end paths of the channel with magnitude larger than a fraction of the channel maximum magnitude. In other words, any multipath components before T_l and after T_h are smaller than $s \cdot \max(|\alpha_k|_{k=0}^{K-1})$, where s (= 0.3 in the simulation) is the scale factor and α_k is the k-th path gain.

Fig. 3.3 shows that at BER = 10^{-3} in CM1 channels, TR pulse cluster outperforms NC-PPM with "+1" pulses by about 1.9 dB, and NC-PPM with "-1" pulses by about 1.3 dB. The performance gap between TRPC and the conventional TR is wider at medium SNRs because of the noise reduction in TRPC due to short integration intervals. At higher SNRs, the IPI effect is more dominant and hence the performance gain mainly comes from the extra energy collected in TRPC. The relative performance between non-coherent detection with "+1" pulse cluster and "-1" pulse cluster is channel dependent. Fig. 3.4 shows that in CM8 channels, TRPC outperforms NC-PPM with "+1" pulses by about 2.3 dB and NC-PPM with "-1" pulses by about 1.3 dB at BER = 2×10^{-3}. The conventional TR scheme significantly lags behind the new TRPC scheme in terms of performance and implementation. This indicates that the extra energy collected by TRPC over TR, and the noise reduction and ISI reduction due to its compact structure exceed the penalty caused by inter-pulse

interference. The performance gain of TRPC in CM8 NLOS channels is larger than in CM1 channels since CM8 channels are more sparsely spread over longer time duration and hence result in less IPI and more noise reduction. Both figures demonstrate agreement between semi-analytical and simulation results for the performances of TRPC and non-coherent PPM schemes.

Fig. 3.5 plots the effect of T_d on the performance of TRPC and non-coherent systems in CM1 and CM8 channels, respectively. These are the simulation results obtained with 1000 channel realizations. In general, the gaps among using different T_d's are not significant. At high SNRs ($>$ 16 dB), $T_d = 5T_p$ slightly outperforms $T_d = T_p$, especially in CM8 channels. This figure indicates that shorter delay lines such as T_p-long is preferred in TRPC and the benefit brought by larger T_d is not obvious.

A practical imperfect factor at implementation is the delay offset between receiver and transmitter. Since TRPC requires delay lines on the order of a few pulse widths, accurate short delay is much easier to realize than long wideband delays. Moreover, the delay offset can be minimized at the manufacturing stage as long as the transmitter and the receiver use the same length delay lines. Fig. 3.6 shows the effect of delay offset on the performance of TRPC. When the receiver delay T_d is $\frac{1}{16}T_p$ longer than the T_p delay used in the transmitter, a small degradation is incurred in CM1 channels. The degradation is about 0.3 dB in CM8 channels at BER $= 10^{-3}$.

Fig. 3.7 presents the effect of N_f on the performance of TR pulse cluster system in CM1 and CM8 channels. As mentioned before, N_f is the repetition times of the reference-data pulse pairs. It is observed that in both channels, the best performance is achieved when $N_f = 4$. As expected, an N_f as large as 8 leads to poorer perfor-

mance than a smaller N_f (such as 4 or 6) because of the noise effect. On the other hand, $N_f = 2$ underperforms $N_f = 4$ because the former collects $3/4E_b$ and the latter get $7/8E_b$ in the receiver, as shown in (3.3). Moreover, the fact that the curves of $N_f = 2$ and $N_f = 8$ in CM1 channels cross can be explained similarly. Recall that the integration length is approximately the length of the channel containing significant energy plus the cluster width. In CM1 channels, the width of a cluster with a large N_f can be often larger than the significant channel length. The $N_f = 2$ curve outperforms $N_f = 8$ at low to medium SNRs because the smaller cluster width at $N_f = 2$ leads to much shorter integration interval than $N_f = 8$ and hence less noise included in the decision statistics. When SNR is medium or low, the TRPC performance is dominated by the noise effect and therefore $N_f = 2$ leads to better performance than $N_f = 8$. As SNR increases, the noise effect is less pronounced. According to eq. (3.3), $N_f = 8$ results in $15/16E_b$ energy collected, compared to $3/4E_b$ for $N_f = 2$. Therefore $N_f = 2$ has worse bit error rate than $N_f = 8$ at high SNRs.

Fig. 3.8 compares the BER performance of TRPC and FSR in CM1, CM4 and CM8 channels. CM4 models office NLOS environments and the data rate simulated is 1Mbps. For fair comparison, the peak power and the average power of both schemes are set to be equal, which leads to $N_{f,FSR} = 6N_{f,TRPC} = 24$ [17]. It is shown in Fig. 3.8 that TRPC outperforms FSR in all three types of channels. The building blocks of the TRPC and FSR receivers are very similar, except that the short delay line in TRPC is replaced by a mixer in FSR.

3.3 Summary

TRPC structure that consists of a group of identical dual pulses with uniform spacing is proposed. This method allows a simple and robust receiver to be implemented, i.e., analog front end, symbol rate sampling and short delay lines, overcoming a major hurdle (long delay line requirement) of conventional TR receivers. Simulation results have shown superior performance of the proposed scheme over non-coherent PPM with energy detection, conventional TR and frequency shifted reference systems in multipath UWB channels.

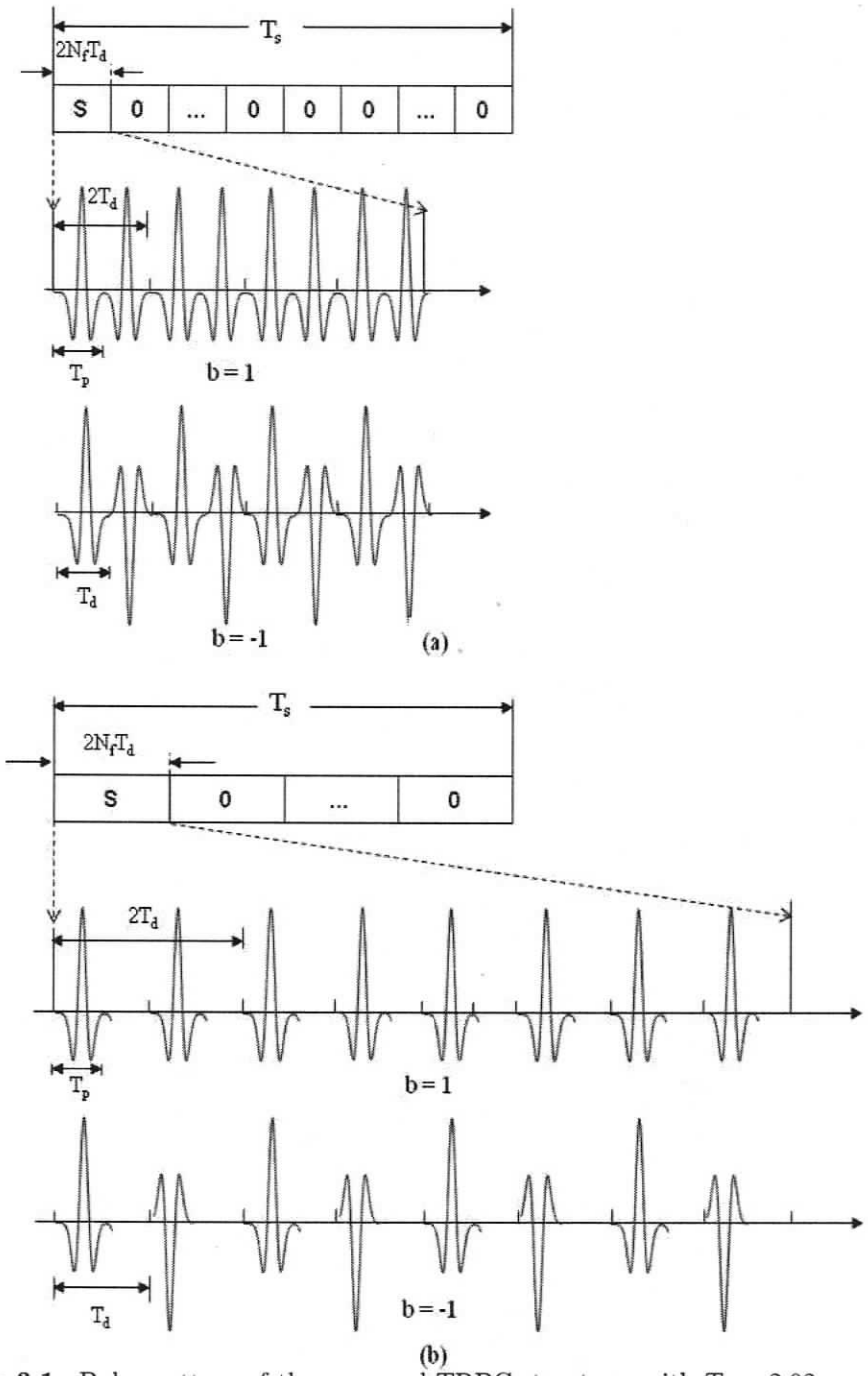

Figure 3.1: Pulse pattern of the proposed TRPC structure, with $T_p = 2.02\ ns$, $N_f = 4$; $T_d = T_p$ in subplot (a) and $T_d = 2T_p$ in subplot (b).

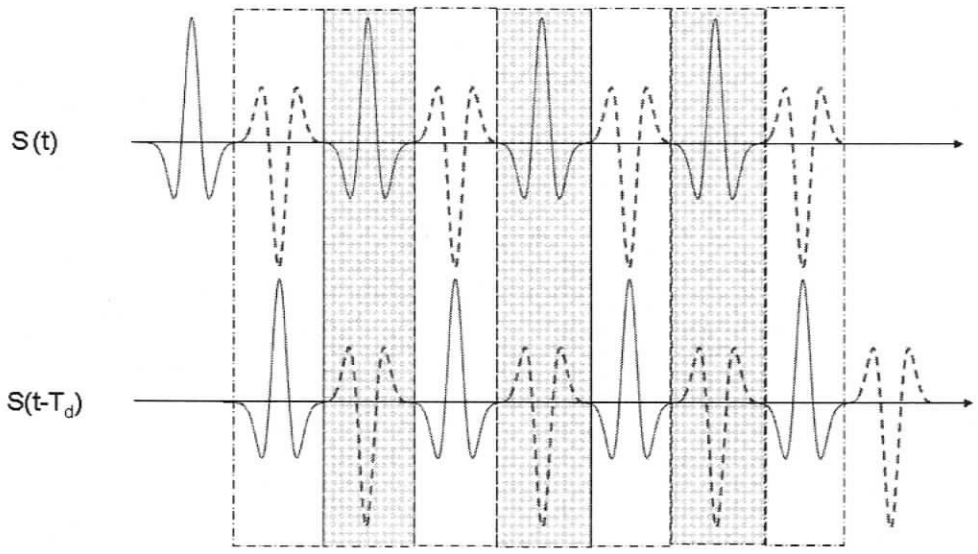

Figure 3.2: Energy collection in the receiver of the proposed TRPC system

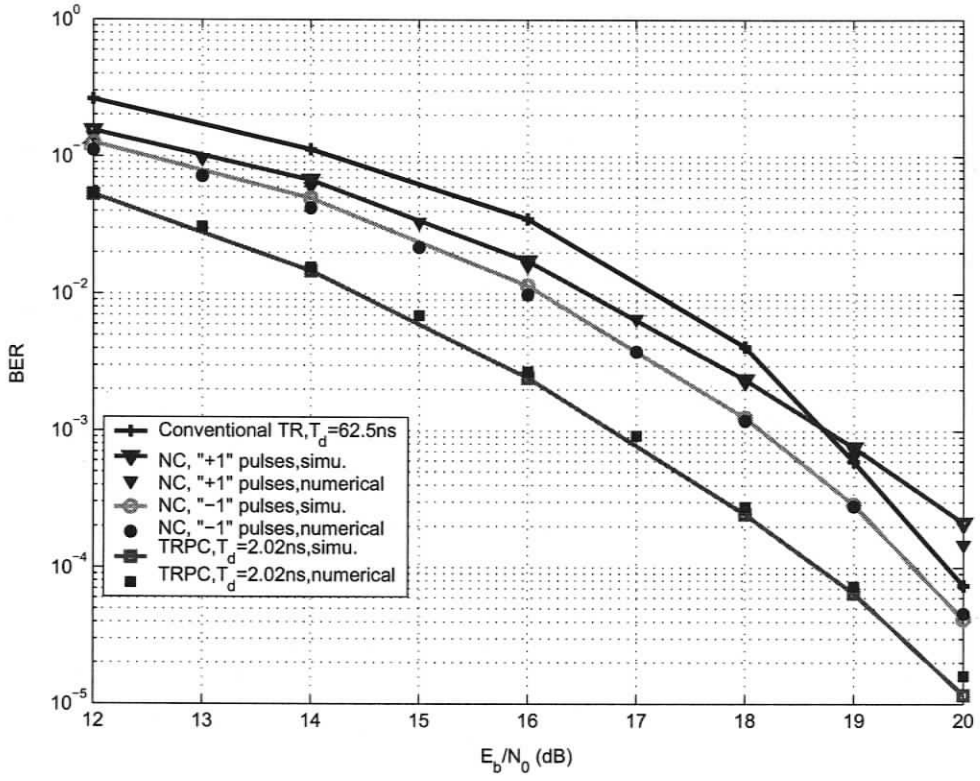

Figure 3.3: The BER of TRPC and non-coherent systems in CM1 channels, with $N_f = 4$.

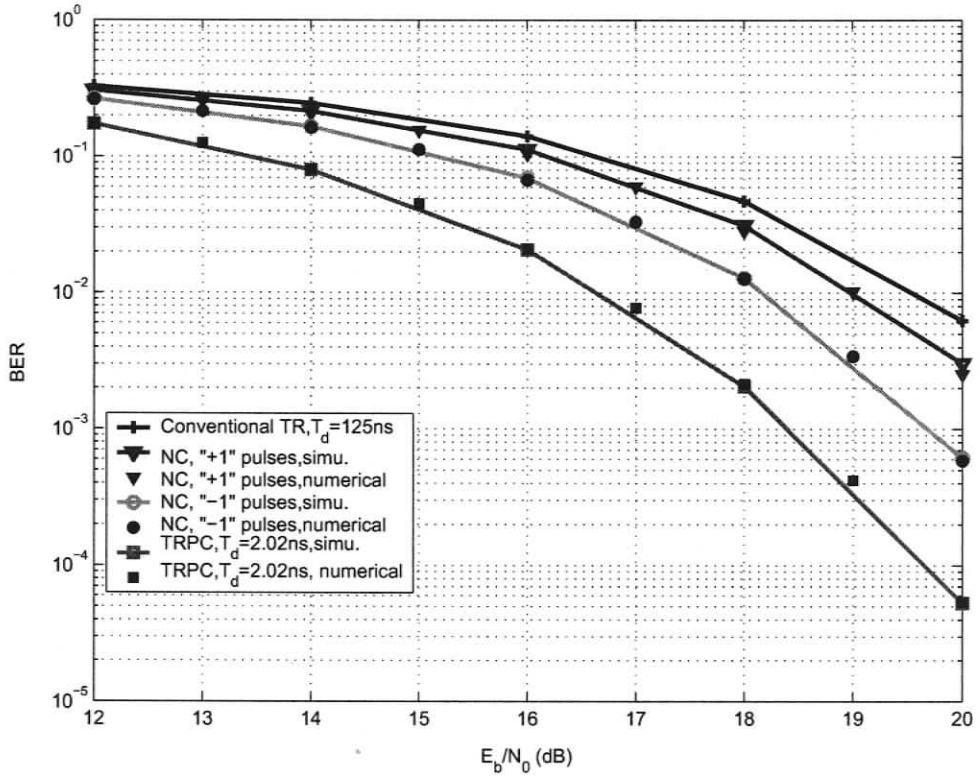

Figure 3.4: The BER of TRPC and non-coherent systems in CM8 channels, with $N_f = 4$.

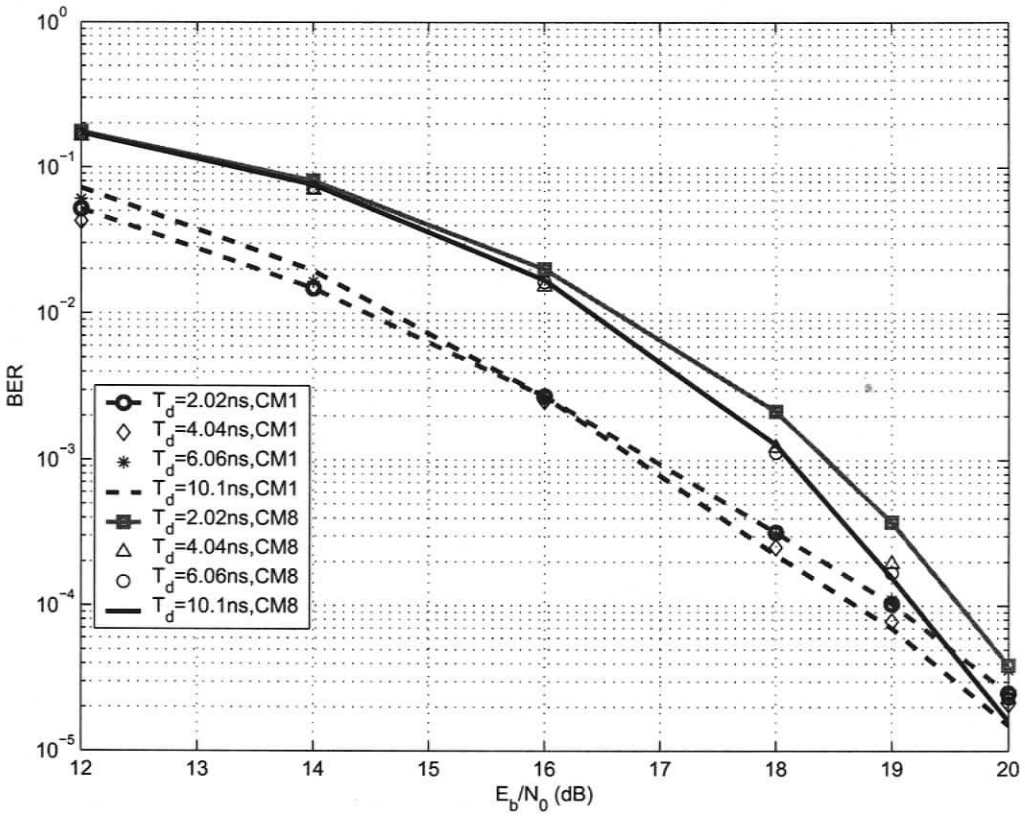

Figure 3.5: The BER of TRPC systems with different T_ds in CM1 and CM8 channels.

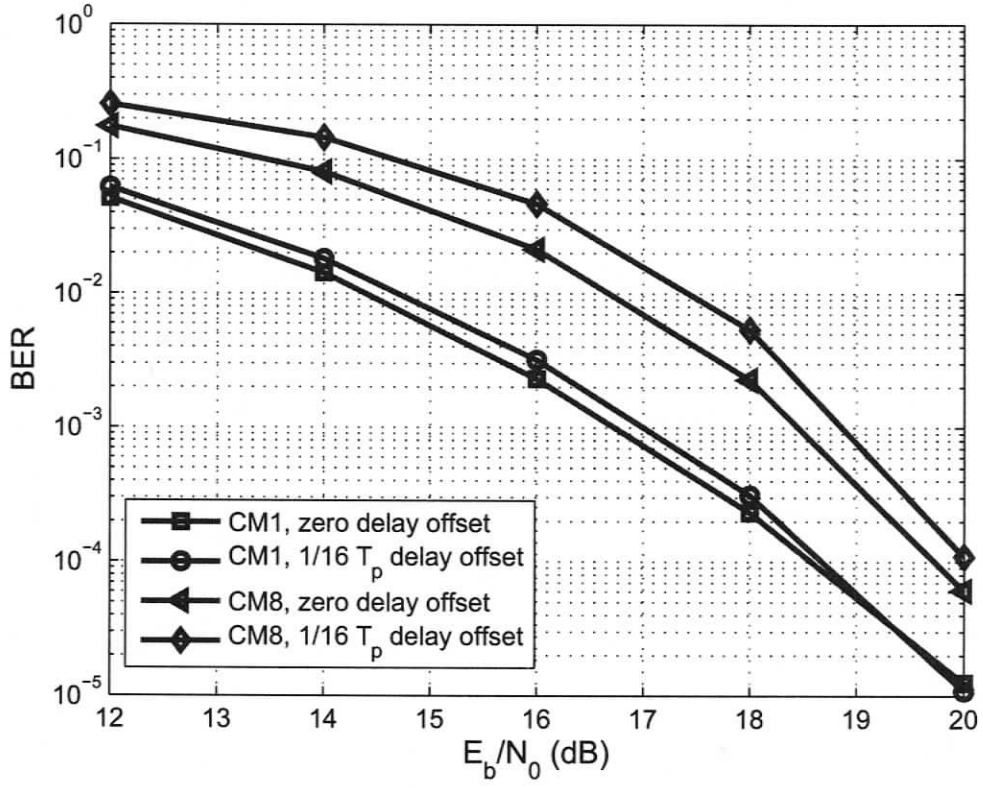

Figure 3.6: The effect of delay offset on the BER of TRPC systems in CM1 and CM8 channels.

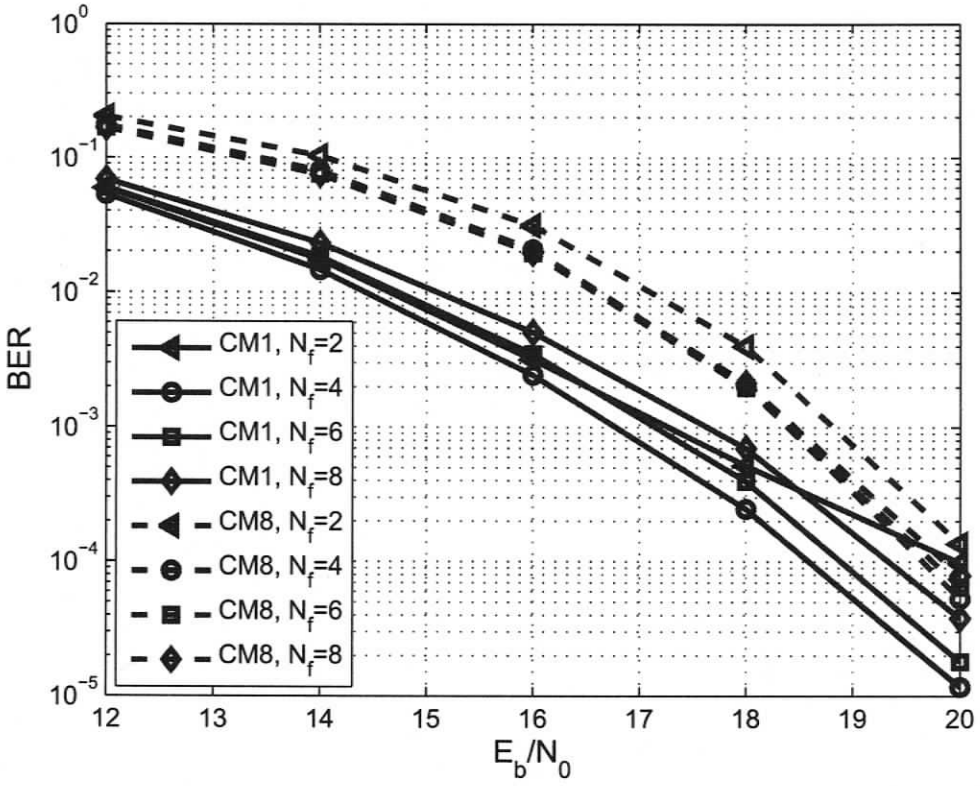

Figure 3.7: The BER of TRPC in CM1 and CM8 channels with different N_fs.

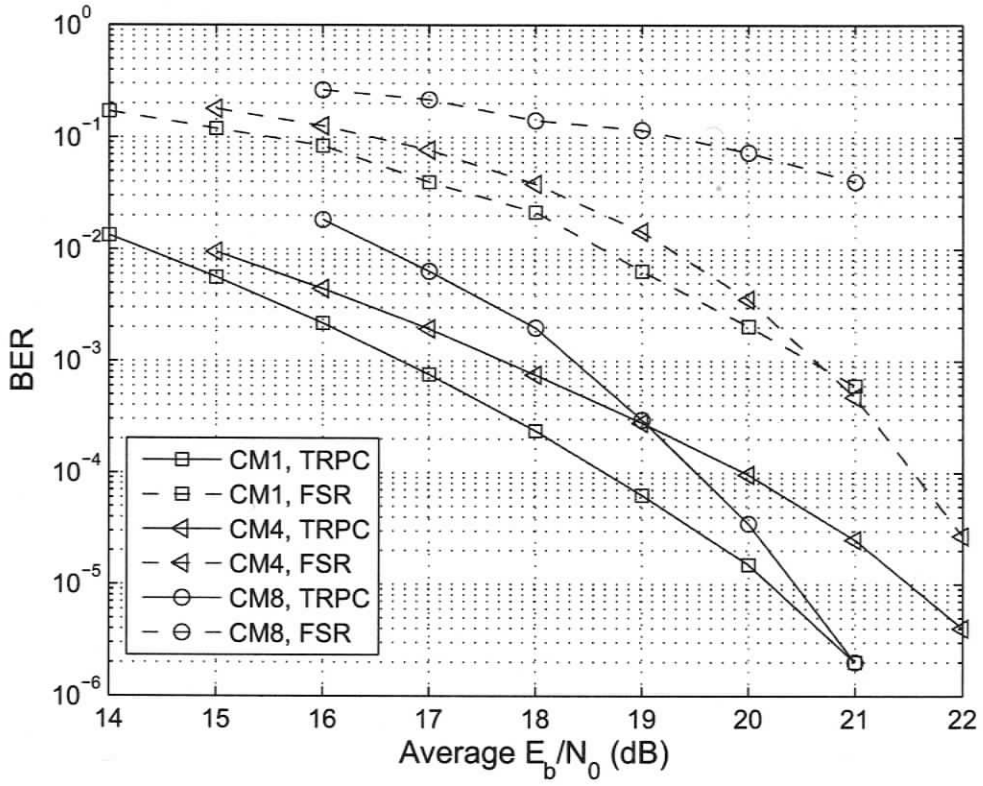

Figure 3.8: Comparison of the BERs of TRPC and FSR in CM1, CM4 and CM8 channels.

Chapter 4

Integration Interval Determination in Transmitted Reference Pulse Cluster Systems for UWB Communications

4.1 Background

In Chapter 3, the detection of TRPC signal is based on an assumption that the detector is equipped with sufficient channel information to determine the beginning and the end of the integration. However, in real systems knowledge of this kind can become extremely difficult to obtain. On the other hand, even if the channel information is known to the receiver, determining the best integration interval is still not a trivial problem. Intuitively, too short an integration intervals cannot cover the span of the UWB channel impulse response and thus fail to collect sufficient energy, while excessive integration length will inevitably add more noise and deteriorate the performance. The objective of this chapter is to find an applicable way to locate the most suitable integration interval for TRPC systems, with no prior channel information.

Integration interval determination in different *conventional* TR type detectors has been studied in [5, 10, 24–28]. A hybrid matched filter correlation receiver was presented in [24] with the fixed integration length $T_{int} = 15$ ns used for IEEE 802.15.3a channel models 1 and 4. This integration interval was further optimized for inter-frame interference (IFI) free transmission in [25] to minimize the bit-error-probability (BEP). As suggested in [10] and [5], the performance improvement brought by increasing the integration time for the TR autocorrelation receiver start to diminish after $T = 20$ ns and $WT = 40$, for the channels studied in the papers. A maximum likelihood (ML) template and generalized likelihood ratio test (GLRT) receivers were used in [26] and by maximizing the effective signal-to-noise ratio (SNR), the optimized number of samples for integration was obtained. Note that Nyquist rate sampling was required in [26]. In [27], the autocorrelation intervals were divided into smaller sub-intervals and those sub-intervals were linearly combined by properly choosing weights to reduce the noise effect. In [28], a practical algorithm was proposed to optimize the integration intervals for the conventional TR systems based on BER minimization. It should be pointed out that all these work were based on the conventional inter-frame interference and inter-pulse interference (IPI) free TR structures which require rather long delay lines in the receivers. So far no literature has dealt with the integration interval determination of the TRPC structure which has its own distinctive characteristics not present in the TR structures. In this chapter, new practical algorithms are developed to determine the integration interval for the TRPC structure. These unique algorithms can be implemented with lower than Nyquist sampling rates and only require short delay lines of a pulse width.

The rest of the chapter is organized as follows: The detailed mathematical deriva-

tions of simplified BER expression for TRPC system are given in Section 4.2. Based on the derivation, three methods are presented, simulated and decided on in Section 4.3 and Section 4.4. Section 4.5 summarizes the chapter.

4.2 Theoretical BER Expression of TRPC System

As described in Chapter 3, in TRPC system, the detector performs correlation on the received signal and its T_d delayed version. The decision variable (DV) for the m-th bit is then given by

$$D(t_b, t_e|b_m) = \int_{mT_s+t_b}^{mT_s+t_e} r(t)r^*(t-T_d)dt, \tag{4.1}$$

where t_b and t_e are the beginning and end of the integration interval. The receiver makes a decision on "+1" if $\mathrm{Re}\{D(t_b, t_e|b_m)\} > 0$, and "-1" if $\mathrm{Re}\{D(t_b, t_e|b_m)\} < 0$. The decision variable can be approximated as a Gaussian RV and the mean of $\mathrm{Re}\{D(t_b, t_e|b_m)\}$ is [29]

$$\mu(t_b, t_e|b_m) = \mathrm{E}\left[\mathrm{Re}\{D(t_b, t_e|b_m)\}\right] = \frac{E_b}{2N_f}\int_{t_b}^{t_e} \mathrm{Re}\{q_{b_m}(t)q^*_{b_m}(t-T_d)\}dt. \tag{4.2}$$

Following the analysis in [29], the variance of $\mathrm{Re}\{D(t_b, t_e|b_m)\}$ is written as

$$\mathrm{Var}[\mathrm{Re}\{D(t_b, t_e|b_m)\}] = \sigma^2_{23}(t_b, t_e|b_m) + \sigma^2_4(t_b, t_e) \tag{4.3}$$

with the mathematical expression of $\sigma_{23}^2(t_b, t_e|b_m)$ and $\sigma_4^2(t_b, t_e)$ are given by

$$\begin{aligned}\sigma_{23}^2(t_b, t_e|b_m) &= \frac{E_b N_0}{4N_f}\int_{t_b}^{t_e}\int_{t_b}^{t_e} \mathrm{Re}\{q_{b_m}(t)q_{b_m}^*(t')\}R_{tr}(t'-t)dtdt' \\ &+ \frac{E_b N_0}{4N_f}\int_{t_b}^{t_e}\int_{t_b}^{t_e} \mathrm{Re}\{q_{b_m}(t-T_d)q_{b_m}^*(t'-T_d)\}R_{tr}(t'-t)dtdt' \\ &+ \frac{E_b N_0}{2N_f}\int_{t_b}^{t_e}\int_{t_b}^{t_e} \mathrm{Re}\{q_{b_m}(t)q_{b_m}^*(t'-T_d)\}R_{tr}(t'-t+T_d)dtdt', \quad (4.4)\end{aligned}$$

and

$$\sigma_4^2(t_b, t_e) = \frac{1}{2}\mathrm{E}\{\int_{t_b}^{t_e}\int_{t_b}^{t_e} n(t)n^*(t-T_d)n^*(u)n(u-T_d)dtdu\}. \quad (4.5)$$

One of the objectives of this chapter is to simplify the bit error rate expression in [29] with approximations so that we can design an integration interval determination algorithm based on the minimum BER. Towards this goal, as shown in Appendix A and Appendix B, $\sigma_{23}^2(t_b, t_e|b_m)$ and $\sigma_4^2(t_b, t_e)$ can be further simplified to

$$\sigma_4^2(t_b, t_e) \approx \frac{N_0^2}{2}(t_e - t_b)\int_{-T_p}^{T_p} R_{tr}(\tau)^2 d\tau = (t_e - t_b)\cdot Y \cdot N_0^2 \quad (4.6)$$

$$\sigma_{23}^2(t_b, t_e|b_m) \approx 2N_0|\mu(t_b, t_e|b_m)|, \quad (4.7)$$

where $Y = \frac{1}{2}\int_{-T_p}^{T_p} R_{tr}(\tau)^2 d\tau$ can be calculated before offline.

Combining (4.6), (4.7) with (4.8), the variance of the decision variable of TRPC system is simplified to

$$\mathrm{Var}[\mathrm{Re}\{D(t_b, t_e|b_m)\}] = \sigma_{23}^2(t_b, t_e|b_m) + \sigma_4^2(t_b, t_e) \approx 2N_0 \cdot |\mu(t_b, t_e|b_m)| + (t_e - t_b)\cdot Y \cdot N_0^2. \quad (4.8)$$

The conditional BER on bit b_m is then given by

$$P(e|\mathbf{h}, b_m, t_b, t_e) \approx Q\left(\frac{|\mu(t_b, t_e|b_m)|}{2N_0 \cdot |\mu(t_b, t_e|b_m)| + (t_e - t_b) \cdot Y \cdot N_0^2}\right). \tag{4.9}$$

4.3 Integration Interval Determination of the TRPC System

In this section, we first explain the asymmetric error rates given by (4.9) conditional on b_m, and describe a training method to determine the dominant data for a particular channel. Then three practical methods are presented to determine the integration interval of the auto-correlation receiver.

4.3.1 Determine the dominant data for the target channel

As the mathematical derivation showed in (4.9), in a TRPC system, the conditional BER of bit +1 and -1 can be distinctive. Therefore the best integration interval for the two bits are different. Since it is impossible to use two integration intervals for one channel, we have consider only one bit instead of both, which is the reason why finding the dominant data is important to our scheme. By optimizing the integration region for the dominant data, it is expected the overall performance will be improved.

The criterion of determining the dominant data d can be expressed as

$$|\mu(t_b, t_e| + 1)| \underset{d=-1}{\overset{d=1}{\lesssim}} |\mu(t_b, t_e| - 1)|. \tag{4.10}$$

Since we shall have $\mu(t_b, t_e| + 1) > 0$ and $\mu(t_b, t_e| - 1) < 0$ to make correct decisions,

(4.10) is simplified to

$$d = -\text{sgn}\{\mu(t_b, t_e| + 1) + \mu(t_b, t_e| - 1)\}. \tag{4.11}$$

By substituting (4.2) into (4.11) and integrating over the entire symbol duration $[0, T_s]$, since the interval $[t_b, t_e]$ is not known yet, we have

$$d = -\text{sgn}\left\{\text{Re}\{\int_0^{T_s} q_{+1}(t)q_{+1}^*(t - T_d) + q_{-1}(t)q_{-1}^*(t - T_d)dt\}\right\}. \tag{4.12}$$

To simplify (4.12), we first define a signal pattern $x(t) = \sum_{i=0}^{N_f-1} g(t - 2iT_d)$. Because $x(t)$ can be viewed as TRPC structure with only reference pulses, it is named half-TRPC structure. Therefore, the TR "+1" and "-1" pulse clusters can be written as $s_{+1}(t) = x(t) + x(t - T_d)$ and $s_{-1}(t) = x(t) - x(t - T_d)$, respectively. After the two signals pass though the multipath channel $h(t)$, we obtain $q_{+1}(t) = y(t)+y(t-T_d)$ and $q_{-1}(t) = y(t) - y(t - T_d)$, with $y(t) = x(t) \otimes h(t) = \sum_{i=0}^{N_f-1} \sum_{k=0}^{K-1} \alpha_k g(t - 2iT_d - \tau_k)$. Consequently, the integral in (4.12) is written as

$$\begin{aligned}
& \int_0^{T_s} q_{+1}(t)q_{+1}^*(t - T_d) + q_{-1}(t)q_{-1}^*(t - T_d)dt \\
= & \int_0^{T_s} [y(t) + y(t - T_d)][y^*(t - T_d) + y^*(t - 2T_d)] \\
& +[y(t) - y(t - T_d)][y^*(t - T_d) - y^*(t - 2T_d)]dt \\
= & \ 2\int_0^{T_s} y(t)y^*(t - T_d)dt + 2\int_0^{T_s} y(t - T_d)y^*(t - 2T_d)dt \\
= & \ 4\int_0^{T_s} y(t)y^*(t - T_d)dt
\end{aligned} \tag{4.13}$$

where the last equality is justified because the integration interval $[0, T_s]$ covers the

whole span of $y(t)$, $y(t-T_d)$ and $y(t-2T_d)$. Therefore, the dominant data can be determined as

$$d = -\text{sgn}\left\{\text{Re}\{\int_0^{T_s} y(t)y^*(t-T_d)dt\}\right\}. \tag{4.14}$$

Compared to (4.12), (4.14) only involves one signal structure $y(t)$, instead of both $q_{+1}(t)$ and $q_{-1}(t)$ in (4.12). Since $y(t)$ in (4.14) is noise free and not obtainable, we can only estimate $y(t)$ from the received signal through noise averaging. The training sequence is thus designed as

$$f_1(t) = \sqrt{\frac{E_b}{2N_f}} \sum_{m=0}^{N_1-1} x(t-mT_s) \tag{4.15}$$

where N_1 is the training length. After the training sequence passes through the multipath channel, the received signal is written as

$$r_1(t) \;=\; \sqrt{\frac{E_b}{2N_f}} \sum_{m=0}^{N_1-1} y(t-mT_s) + n(t). \tag{4.16}$$

Following (4.14), the receiver performs the integration-and-dump (I&D) procedure every T_s seconds and obtains

$$\chi_m = \text{Re}\{\int_{mT_s}^{(m+1)T_s} r_1(t)r_1^*(t-T_d)dt\}, \quad m = 0, 1, \ldots, N_1 - 1. \tag{4.17}$$

Finally the dominant data can be determined as

$$d = -\text{sgn}\{\frac{1}{N_1}\sum_{m=0}^{N_1-1}\chi_m\} = -\text{sgn}\{\sum_{m=0}^{N_1-1}\chi_m\}. \tag{4.18}$$

For the transmitter to know the dominant data, either the receiver feedbacks

this information to the transmitter or the receiver (instead of the transmitter) sends the training sequence and the transmitter determines the dominant data from the received training sequence. The latter approach relies on the channel reciprocity property, which has been verified by our extensive measurement experiments [30]. Another alternative is to use one sufficiently long training sequence consisting of "+1" and "-1", bypassing the second training sequence of the next subsection consisting of the dominant data only. The receiver first determines the dominant data from this training sequence and then uses the corresponding training symbols to determine the integration interval.

4.3.2 Determine the integration interval

To obtain the integration interval for the target channel, a training sequence $f_2(t)$ adopting TRPC structure with dominant data d is applied. That is,

$$f_2(t) = \sqrt{\frac{E_b}{2N_f}} \sum_{m=0}^{N_2-1} s_d(t - mT_s), \tag{4.19}$$

where N_2 is the training length. After it goes through the channel, the received signal can be written as

$$r_d(t) = f_2(t) * h(t) + n(t) = \sqrt{\frac{E_b}{2N_f}} \sum_{m=0}^{N_2-1} q_d(t - mT_s) + n(t). \tag{4.20}$$

After the received signal passes through low-noise amplifier (LNA) and matched filter (MF), it is first multiplied with its T_d delayed version, then put through I&D device and sampled over subintervals of Δ seconds, as shown in Fig. 4.1. The total number of samples is $T_s/\Delta \times N_2$. The auto-correlation over the i-th bin/subinterval in the

m-th training symbol is calculated as

$$X_m[i] = \int_{mT_s+(i-1)\Delta}^{mT_s+i\Delta} r_d(t) r_d^*(t - T_d) dt, \quad i = 1, 2, ..., T_s/\Delta; \quad m = 1, 2, ..., N_2. \quad (4.21)$$

Next we will present three different algorithms to locate the beginning and end points of the integration interval, all based on the bin auto-correlation results given by (4.21).

1) The Conventional Threshold-crossing Method

Similar to the conventional energy detection with threshold-crossing method, the adapted version for TRPC is given as follows. To mitigate the noise effect, the auto-correlation in each bin is first averaged over the training length to get

$$Z[i] = \frac{1}{N_2} \sum_{m=1}^{N_2} X_m[i], \quad i = 1, 2, ..., T_s/\Delta. \quad (4.22)$$

Based on the averaged bin auto-correlation, a threshold Z_{th} is defined as

$$Z_{th} = \xi \cdot Z_{max} = \xi \cdot \max_{1 \le i \le T_s/\Delta} Z[i] \quad (4.23)$$

where $\xi (0 < \xi < 1)$ is referred to as the normalized threshold. Therefore, the beginning (t_b) and end (t_e) are determined as the first and last bins exceeding the threshold Z_{th}, that is,

$$\begin{aligned} \hat{\phi}_b &= \arg\min_i Z[i] > Z_{th} \\ \hat{\phi}_e &= \arg\max_i Z[i] > Z_{th}. \end{aligned} \quad (4.24)$$

Since $\hat{\phi}_b$ and $\hat{\phi}_e$ are the bin indexes, the actual time for the beginning and end points

of the integration are $\hat{t}_b = \Delta \cdot \hat{\phi}_b$ and $\hat{t}_e = \Delta \cdot \hat{\phi}_e$, respectively.

In summary, the threshold-crossing method first locates the bin with the maximum auto-correlation and then selects the first and last bins that exceed the fixed threshold as the beginning and end points for the integration interval. It aims at including all the multipaths with significant energy (above the absolute threshold) in the received signal to carry out the detection. However, the fixed threshold-exceeding criterion makes it vulnerable to unexpected noise spikes, especially at low SNR scenarios. Meanwhile, the effectiveness of the threshold-crossing method also depends on the threshold value chosen.

2) The BER Minimization Based Method

Since this paper compares different methods based on the actual BER performance, the optimal integration interval should be the one that minimizes the BER. Given the simplified theoretical BER expression in (4.9) and the property of the Q function, minimizing the BER is equivalent to maximizing the received SNR, that is, the argument of Q in (4.9). Therefore, the BER minimization method determines the beginning and ending points of the integration interval as

$$\begin{aligned} [\hat{t}_b, \hat{t}_e] &= \arg\max_{t_b, t_e} \frac{|\mu(t_b, t_e|d)|}{\sqrt{2N_0 \cdot |\mu(t_b, t_e|d)| + (t_e - t_b) \cdot Y \cdot N_0^2}} \\ &= \arg\max_{t_b, t_e} \frac{|\mu(t_b, t_e|d)|}{\sqrt{2|\mu(t_b, t_e|d)|/N_0 + (t_e - t_b) \cdot Y}} \end{aligned} \tag{4.25}$$

To estimate $\mu_d(t_b, t_e|d)$, the received signal in (4.20) is multiplied with its T_d delayed version, integrated over every symbol long segments, and average the integration

results to obtain

$$\begin{aligned} D(t_b,t_e|d) &= \frac{1}{N_2}\sum_{m=0}^{N_2-1}\int_{mT_s+t_b}^{mT_s+t_e} r_d(t)r_d^*(t-T_d)dt \\ &= \int_{t_b}^{t_e}\frac{1}{N_2}\sum_{m=0}^{N_2-1} r_d(t+mT_s)r_d^*(t-T_d+mT_s)dt = \int_{t_b}^{t_e}\overline{r_d(t)r_d^*(t-T_d)}dt \\ &= \int_{t_b}^{t_e}\Big[\frac{E_b}{2N_f}q_d(t)q_d^*(t-T_d)+\sqrt{\frac{E_b}{2N_f}}q_d(t)\overline{n^*(t-T_d)} \\ &+ \sqrt{\frac{E_b}{2N_f}}q_d^*(t-T_d)\overline{n(t)}+\frac{1}{N_2}\sum_{m=0}^{N_2-1}n(t-mT_s)n^*(t-mT_s-T_d)\Big]dt, \end{aligned} \tag{4.26}$$

where $\overline{n}(t)=\sum_{l=0}^{N_2-1}n(t+mT_s)/N_2 \sim \mathcal{N}(0,BN_0/N_2)$. The purpose of averaging is to reduce the noise variance. Since the last three terms of (4.26) all have zero mean, we have

$$\mathrm{E}[\mathrm{Re}\{D(t_b,t_e|d)\}] \approx \frac{E_b}{2N_f}\int_{t_b}^{t_e}\mathrm{Re}\{q_d(t)q_d^*(t-T_d)\}dt = \mu(t_b,t_e|d). \tag{4.27}$$

Consequently, $\mathrm{Re}\{D(t_b,t_e|d)\}$ is an unbiased estimate for $\mu(t_b,t_e|d)$ with the variance

$$\begin{aligned} \mathrm{Var}[\mathrm{Re}\{D(t_b,t_e|d)\}] &= \frac{E_bN_0}{4N_fN_2}\int_{t_b}^{t_e}\left[|q_d(t)|^2+|q_d(t-T_d)|^2\right]dt \\ &+ \frac{E_bN_0}{2N_fN_2}\int_{t_b}^{t_e}\mathrm{Re}\{q_d^*(t)q_d(t-2T_d)\}dt + \frac{N_0^2}{2N_2}(t_e-t_b)\int_{-T_p}^{T_p}R_{tr}^2(\tau)d\tau \end{aligned} \tag{4.28}$$

which can be improved by increasing N_2. Therefore, by substituting $\mathrm{Re}\{D(t_b,t_e|d)\}$

into (4.25), the integration interval can be finally determined as

$$[\hat{t}_b, \hat{t}_e] = \arg\max_{t_b,t_e} \frac{|\mathrm{Re}\{D(t_b,t_e|d)\}|}{\sqrt{2|\mathrm{Re}\{D(t_b,t_e|d)\}|/N_0 + (t_e - t_b)\cdot Y}}. \tag{4.29}$$

The denominator of (4.29) consists of two terms, where the former, i.e., $2|\mathrm{Re}\{D(t_b,t_e|d)\}|/N_0$ is proportional to the SNR, and the latter only depends on the integration length. When the SNR is low, we may neglect the first part and (4.29) is simplified to

$$[\hat{t}_b, \hat{t}_e] = \arg\max_{t_b,t_e} \frac{|\mathrm{Re}\{D(t_b,t_e|d)\}|}{\sqrt{t_e - t_b}}. \tag{4.30}$$

By this simplification, we can compute the integration interval through (4.30) without the knowledge of N_0. It is expected that this simplification would suffer degradation as SNR increases.

The BER minimization based scheme is suitable for practical implementation because it does not require analog averaging using long wideband delay lines nor digital averaging at Nyquist sampling rate. The continuous time formulation in (4.29) and (4.30) can be implemented using the bin auto-correlation results in (4.21). The bin indexes of the integration interval that minimize the BER are determined as

$$[\hat{\phi}_b, \hat{\phi}_e] = \arg\max_{\phi_b,\phi_e} \frac{|\sum_{m=0}^{N_2-1}\sum_{i=\phi_b}^{\phi_e} X_m[i]|/N_2}{\sqrt{2|\sum_{m=0}^{N_2-1}\sum_{i=\phi_b}^{\phi_e} X_m[i]|/(N_0N_2) + (\phi_e - \phi_b)\Delta\cdot Y}}. \tag{4.31}$$

At low to medium SNRs, the integration interval can be obtained as

$$[\hat{\phi}_b, \hat{\phi}_e] = \arg\max_{\phi_b,\phi_e} \frac{|\sum_{m=0}^{N_2-1}\sum_{i=\phi_b}^{\phi_e} X_m[i]|}{\sqrt{\phi_e - \phi_b}}. \tag{4.32}$$

3) The Hybrid Method

As summarized above, the threshold-crossing method is intuitive and easy to implement, but vulnerable to the noise effect. On the other hand, the BER minimization based method determines the optimal integration interval from theoretical derivation and is thus more accurate. However, it requires a two-dimensional search with a computation complexity of $O(N^2)$ where $N = T_s/\Delta$.

To keep the low complexity characteristics in the threshold-crossing method while at the same time utilizing the accurate integration interval obtained by the BER minimization based method, a hybrid method is proposed in this section, which uses the threshold-crossing method to locate the integration starting point, and applies the one dimensional search method to determine the end point.

Following (4.24) in the threshold-crossing method, the beginning point is determined as

$$\hat{t}_b = \hat{\phi}_b \cdot \Delta = \left\{ \arg\min_i Z[i] > Z_{th} \right\} \cdot \Delta. \tag{4.33}$$

After substituting the beginning point $\hat{t}_b$ into (4.29), we find the ending point of the hybrid method by

$$\hat{t}_e = \arg\max_{t_e} \frac{|\mathrm{Re}\{D(\hat{t}_b, t_e|d)\}|}{\sqrt{2|\mathrm{Re}\{D(\hat{t}_b, t_e|d)\}|/N_0 + (t_e - \hat{t}_b) \cdot Y}}. \tag{4.34}$$

Similarly, when the SNR is low, the first part of the denominator in (4.34) can be ignored and we have

$$\hat{t}_e = \arg\max_{t_e} \frac{|\mathrm{Re}\{D(\hat{t}_b, t_e|d)\}|}{\sqrt{t_e - \hat{t}_b}}. \tag{4.35}$$

In terms of implementation, the ending point of the integration interval is deter-

mined as

$$\hat{\phi}_e = \arg\max_{\phi_e} \frac{|\sum_{m=0}^{N_2-1}\sum_{i=\hat{\phi}_b}^{\phi_e} X_m[i]|/N_2}{\sqrt{2|\sum_{m=0}^{N_2-1}\sum_{i=\hat{\phi}_b}^{\phi_e} X_m[i]|/(N_0N_2) + (\phi_e - \hat{\phi}_b)\Delta \cdot Y}}. \tag{4.36}$$

At low to medium SNRs, the integration interval can be obtained as

$$\hat{\phi}_e = \arg\max_{\phi_e} \frac{|\sum_{m=0}^{N_2-1}\sum_{i=\hat{\phi}_b}^{\phi_e} X_m[i]|}{\sqrt{\phi_e - \hat{\phi}_b}}. \tag{4.37}$$

Compared to (4.31), the hybrid method only requires a one dimensional search for ϕ_e. Thus the total computational complexity is reduced significantly from $O(N^2)$ to $O(N)$.

4.4 Simulation Results

In this section, we present simulation results for the performance of the proposed integration interval determination schemes. The normalized threshold parameter in threshold-crossing method is set to be ξ=0.35, which delivers the best results as shown in Fig. 4.2. Rest of the system setup follows Chapter 3 and will be omitted here for simplicity.

Fig. 4.3 and Fig. 4.4 plot the BER performances of the threshold-crossing [eq. (4.24)], the BER minimization based [(4.31), (4.32)] and the hybrid [(4.36), (4.37)] methods in CM1 and CM8 channels, respectively. Fig. 4.3 shows that in CM1 channels, the BER minimization based method and the hybrid method outperform the threshold-crossing method by 2.0 dB and 1.9 dB, respectively, at BER = 10^{-3}. After omitting the SNR related part in the optimization function, the simplified schemes still save

around 1-1.5 dB compared to the threshold-crossing method. Fig. 4.4 shows in CM8 channels, the BER minimization based method and the hybrid method outperform the threshold-crossing method by 2.0 dB, at BER $= 10^{-3}$. In both channels, the hybrid method achieves similar performance to the BER minimization based method and its simplified version [eq. (4.37)] actually incurs less degradation than the simplified BER minimization based approach [eq. (4.32)] since only the end point search is affected by the simplified optimization function. Furthermore, the simplified schemes suffer more performance degradation at high SNRs in CM8 channels than in CM1 channels, because they tend to locate short intervals which only collect a small part of the signal energy for highly dispersive CM8 channels.

Fig. 4.5 and Fig. 4.6 depict the impact of bin width Δ on the BER performances of the BER minimization based and the hybrid methods. The bin width Δ determines the sampling rate required in the receiver. From the implementation perspective, larger Δ means lower sampling rate and all the benefits brought forth. In CM1 channels, increasing Δ has very little impact on the optimal BER minimization based method. However, for the hybrid method, a performance loss of 2.0 dB in CM1 channels at BER$= 2 \times 10^{-4}$ is observed when Δ increases from 2 ns to 16 ns. In CM8 channels, both schemes have very limited performance loss when Δ increases to 16 ns. Although not shown here, the threshold-crossing method is the most sensitive to the change in Δ. To summarize, the BER minimization based method, followed by the hybrid method, permits lower sampling rate to be used in the receiver than the simple threshold-crossing method. The overall complexity of the receiver then should be carefully considered at the implementation stage.

Figs. 4.7, 4.8 and 4.9 show how the training length N_2 affects the BER per-

formance of the proposed threshold-crossing, the BER minimization based and the hybrid methods in CM1 and CM8 channels. In CM1 channels significant performance degradation is observed in threshold-crossing method by decreasing N_2 from 40 to 10, while on the other hand, the BER minimization based method is not much affected even adopting $N_2 = 10$. In CM8 channels, the training length has little impact on both the threshold-crossing and BER minimization based methods. The performance of the hybrid method is not much affected by varying the training length from $N_2 = 10$ to $N_2 = 40$ in both CM1 and CM8 channels as shown in Fig. 4.9. In summary, both the BER minimization based and hybrid methods are very robust and do not require a long training sequence. On the other hand, the threshold-crossing method needs long training sequence to achieve better results, especially in CM1 channels.

4.5 Conclusion

In this chapter, three new practically implementable algorithms have been proposed to determine the integration interval in the auto-correlation receiver for the TRPC system. Among them, the threshold-crossing method has the lowest complexity but inferior performance, and requires a long training length and relatively high sampling rate. The BER minimization based method has the best BER performance and the lowest requirement on sampling rate and training length but requires a two-dimensional search for the optimal interval. The hybrid method has been shown to yield similar performance to the BER minimization based method in most cases, with much reduced complexity. It is therefore a suitable candidate for a majority of applications.

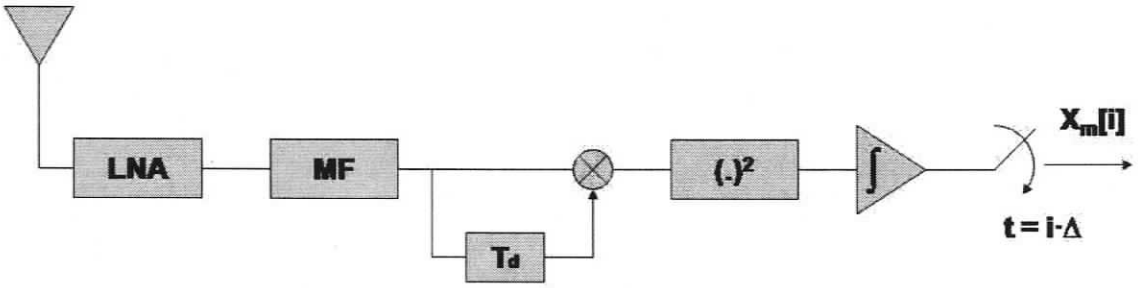

Figure 4.1: Auto-correlation of the received signal.

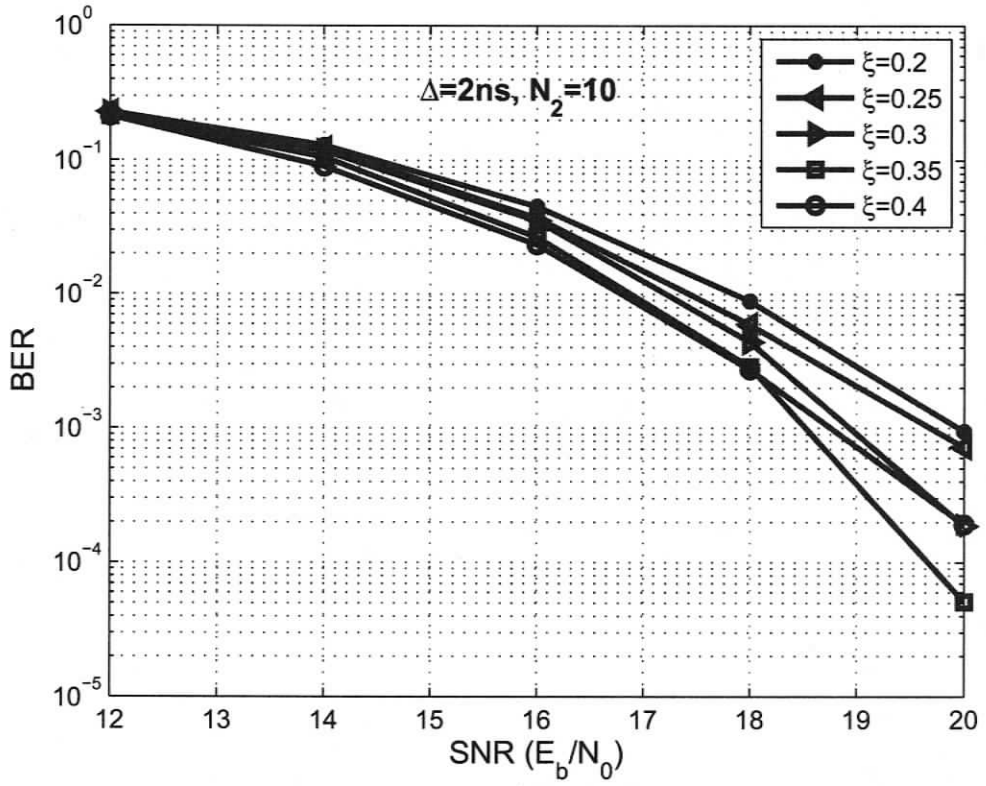

Figure 4.2: BER performance of threshold-crossing method in CM1 channels, with $N_1 = 10$, $N_2 = 10$ and $\Delta = 2$ ns.

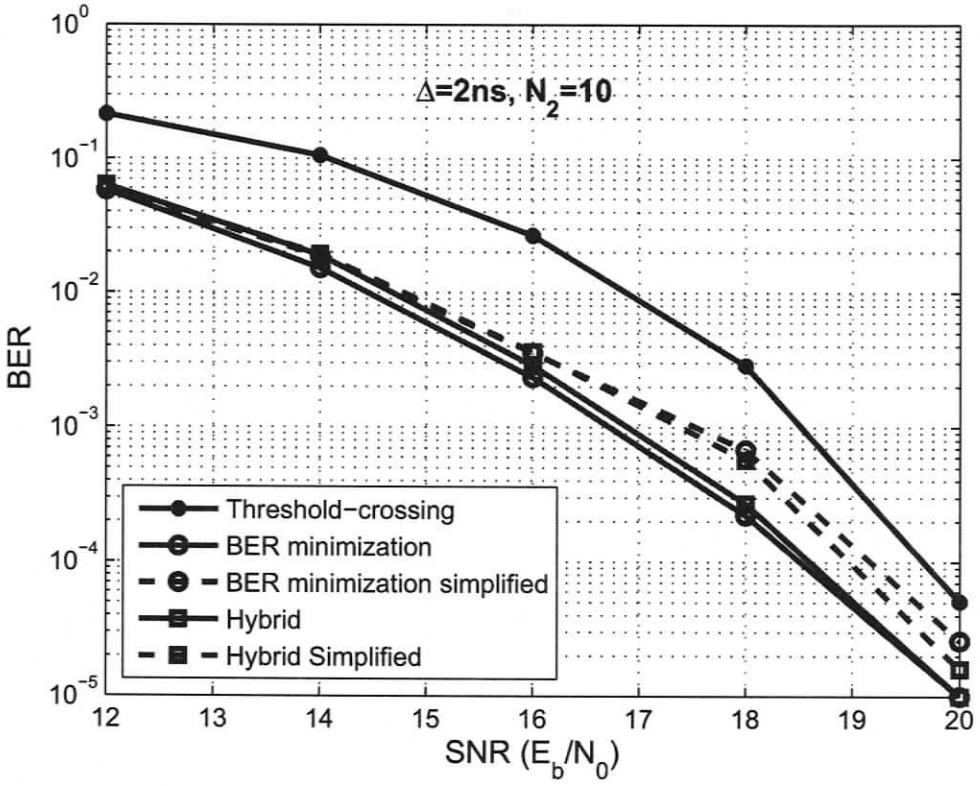

Figure 4.3: BER performance in CM1 channels, with $N_1 = 10$, $N_2 = 10$ and $\Delta = 2$ ns.

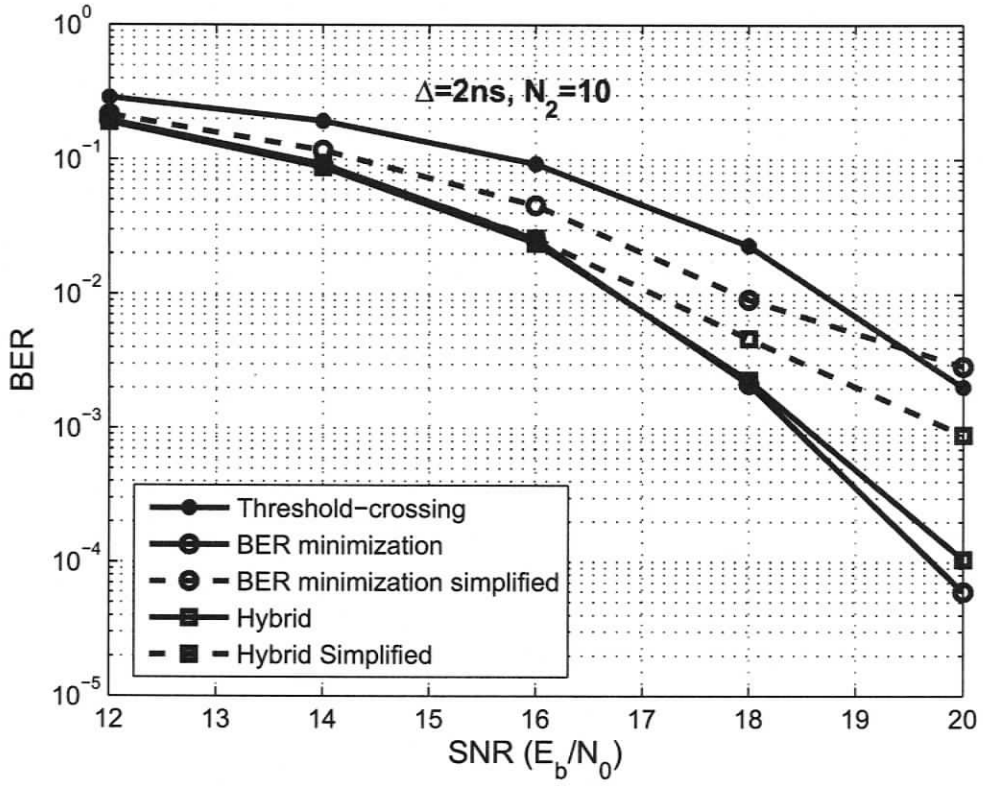

Figure 4.4: BER performance in CM8 channels, with $N_1 = 10$, $N_2 = 10$ and $\Delta = 2$ ns.

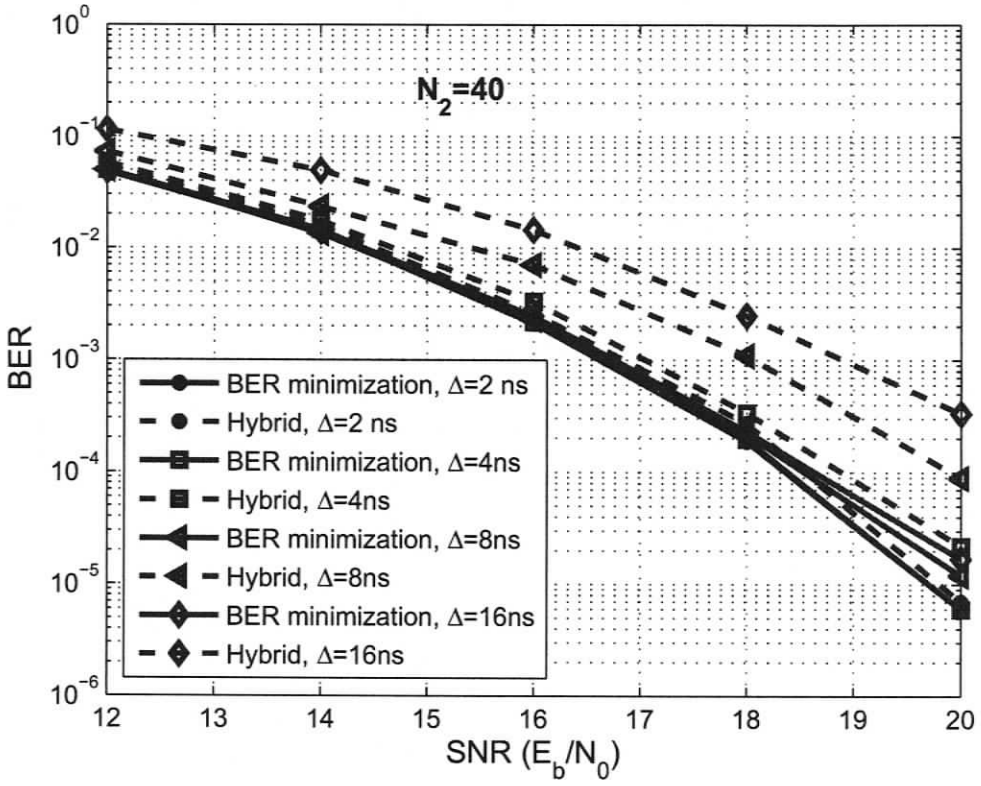

Figure 4.5: The effect of bin width on the BER performance of different integration interval determination methods in CM1 channels, with $N_1 = 10$ and $N_2 = 40$.

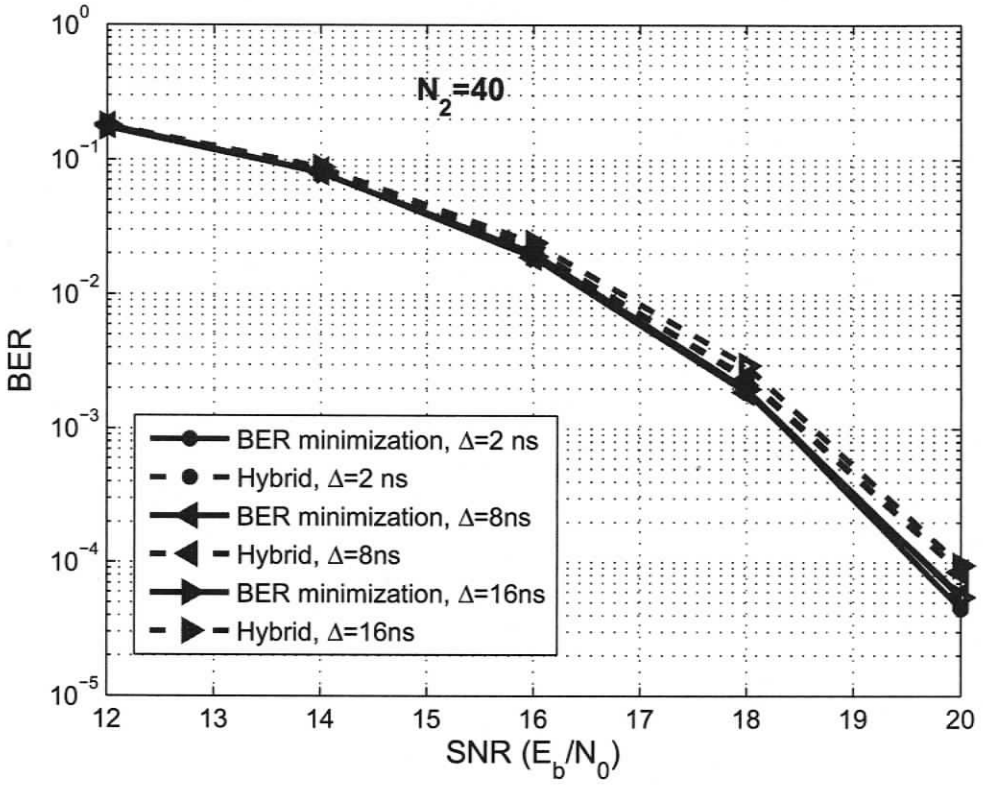

Figure 4.6: The effect of bin width on the BER performance of different integration interval determination methods in CM8 channels, with $N_1 = 10$ and $N_2 = 40$.

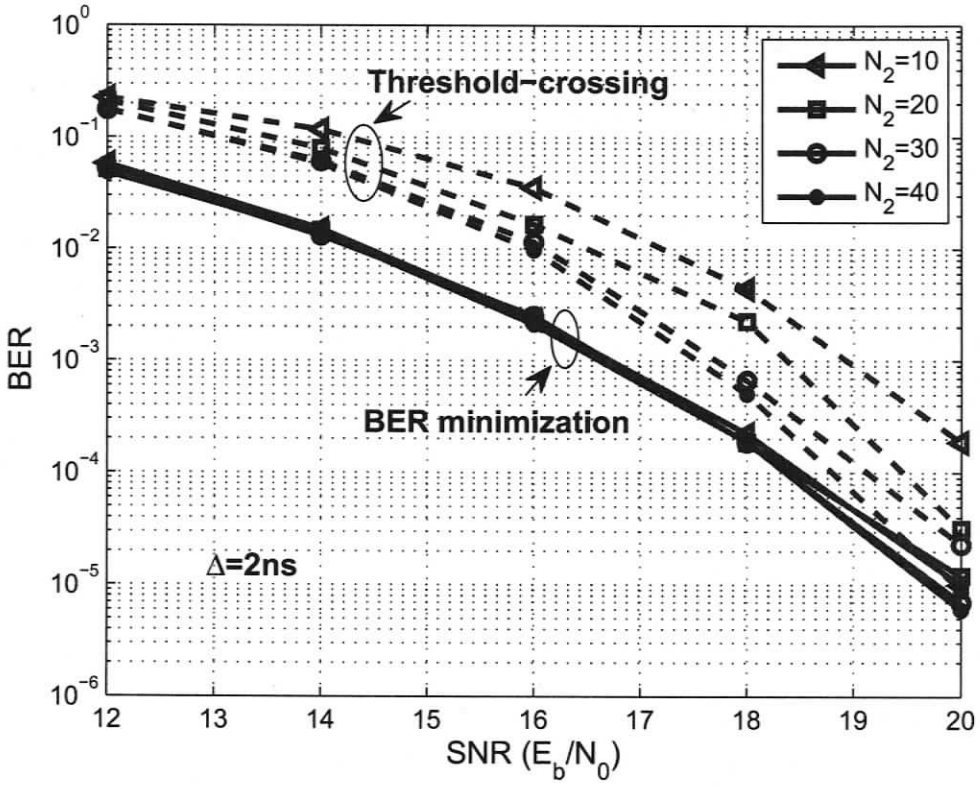

Figure 4.7: Impact of the training length on the threshold-crossing and BER minimization based method in CM1 channels, with $\Delta = 2$ ns.

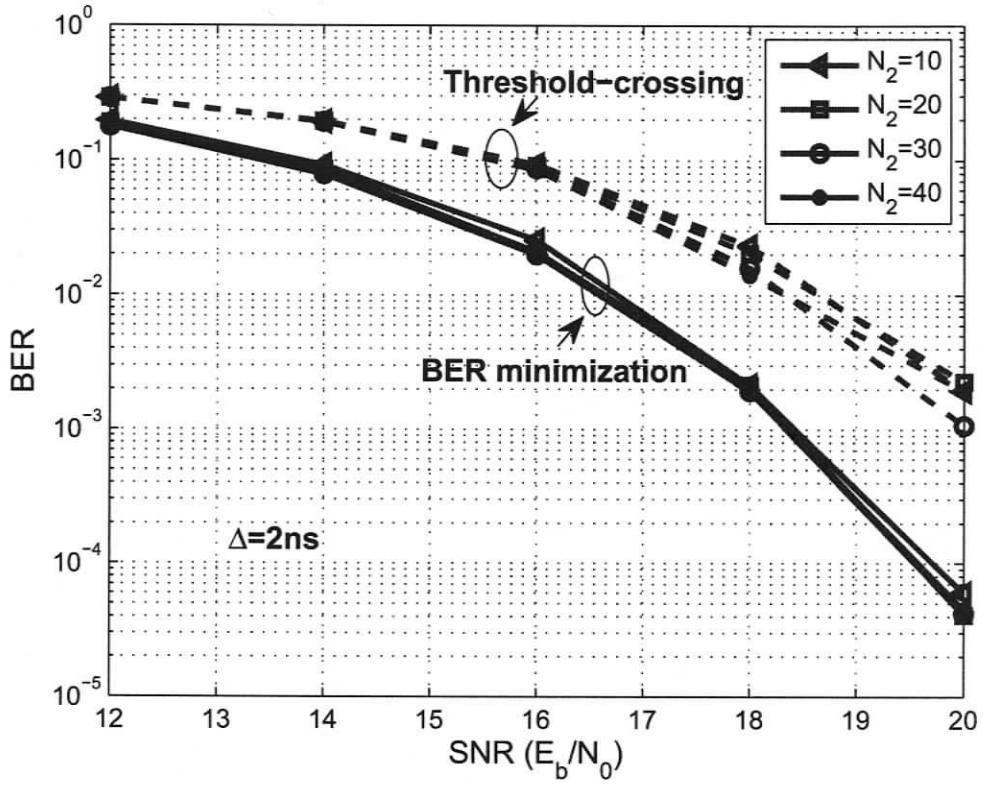

Figure 4.8: Impact of the training length on the threshold-crossing and BER minimization based method in CM8 channels, with $\Delta = 2$ ns.

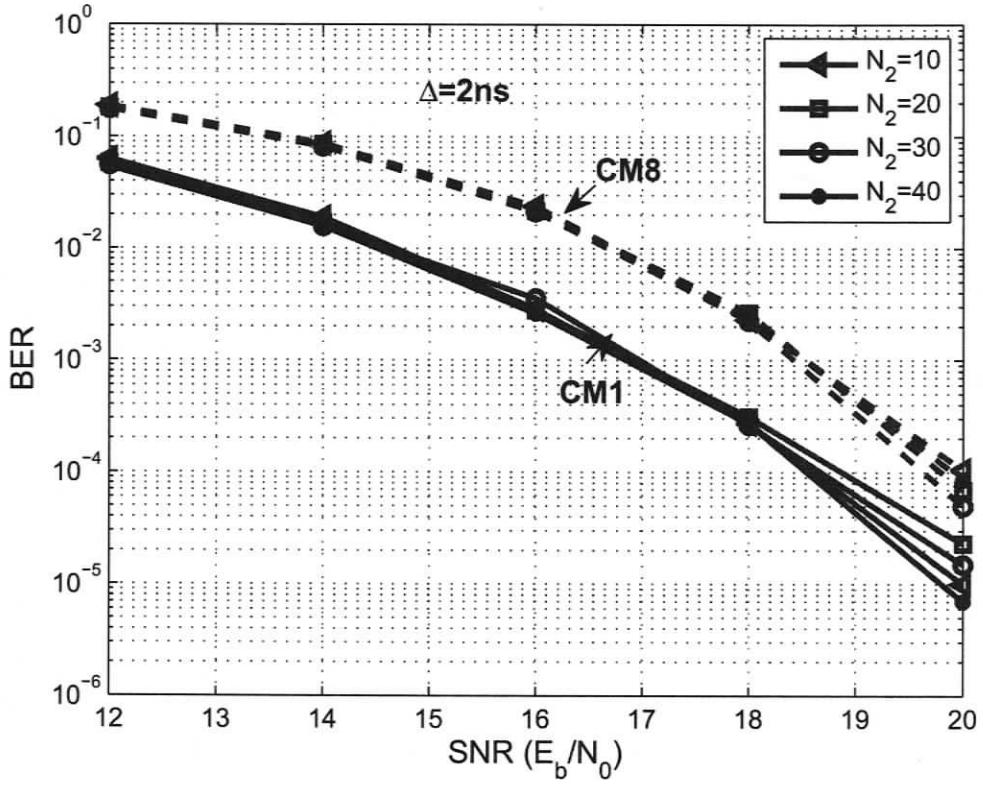

Figure 4.9: Impact of the training length on the hybrid method in CM1 and CM8 channels, with $\Delta = 2$ ns.

Chapter 5

Adaptive Threshold in Transmitted Reference Pulse Cluster System

5.1 Background

When a Gaussian decision variable D has distinct means m_0 and m_1, and equal variance conditional on the equiprobable signal $s_0(t)$ and $s_1(t)$ transmitted, the optimal decision threshold, following the well known communication theory, is then given by $\xi = \frac{m_0+m_1}{2}$. In conventional bipolar systems over additive white Gaussian noise (AWGN) channels, since two signal points are designed to be antipodal, i. e., $m_0 = -m_1$, the optimal threshold is zero. This zero threshold criterion is based on the maximum likelihood (ML) criterion and was adopted in our BPSK detection method for TRPC over UWB channels in Chapter 3.

However, the simulation results of TRPC in Chapter 3 showed a clear disparity in the conditional BER performance when transmitting different bits ("+1" or "-1"). The reason for this asymmetric performance is due to the presence of IPI in the TRPC structure, which makes the two decision variables for bits "+1" and "-1" have

asymmetric mean values with respect to 0. Since m_0 is no longer the opposite of m_1, choosing zero as the decision threshold might not be optimal. This characteristic motivates us to modify the decision threshold and further improve the performance of the TR pulse cluster system.

The rest of the chapter is organized as follows: Section 5.2 reviews the system model of the TRPC system, analyzes the decision variable, and derives the optimal threshold determination mechanism. Then an adaptive threshold scheme is proposed in Section 5.3. Section 5.4 provides with the simulation results and finally the chapter is concluded in Section 5.5.

5.2 System Model and Decision Variable Expectation

Recall from Chapter 3, the TR pulse cluster system has two types of modulated pulse clusters:

$$\begin{aligned} s_{+1}(t) &= \sum_{i=0}^{N_f-1} [g(t-2iT_d) + g(t-(2i+1)T_d)] \\ s_{-1}(t) &= \sum_{i=0}^{N_f-1} [g(t-2iT_d) - g(t-(2i+1)T_d)], \end{aligned} \tag{5.1}$$

where $s_{+1}(t)$ represents the pulse cluster transmitting bit "+1", $s_{-1}(t)$ is the pulse cluster transmitting "-1". After the two pulse clusters go through the multipath channel $h(t)$, defined as $h(t) = \sum_{k=0}^{K-1} \alpha_k \delta(t-\tau_k)$, the the noiseless and inter-symbol

interference (ISI) free received structure are

$$q_{+1}(t) = \sum_{k=0}^{K-1} \alpha_k s_{+1}(t - \tau_k)$$
$$q_{-1}(t) = \sum_{k=0}^{K-1} \alpha_k s_{-1}(t - \tau_k) \tag{5.2}$$

After the transmitted signal goes through the UWB channel $h(t) = \sum_{k=0}^{K-1} \alpha_k \delta(t-\tau_k)$, the received signal is

$$r(t) = \sum_{k=0}^{K-1} \alpha_k \tilde{s}(t - \tau_k) + n(t) = \sqrt{\frac{E_b}{2N_f}} \sum_{m=-\infty}^{\infty} q_{b_m}(t - mT_s) + n(t) \tag{5.3}$$

The decision variable of the m-th bit in the TR pulse cluster system is given by

$$D_m = \int_{t_b+mT_s}^{t_e+mT_s} r(t) r^*(t - T_d) dt = \frac{E_b}{2N_f} \int_{t_b}^{t_e} q_{b_m}(t) q^*_{b_m}(t - T_d) dt + \mathcal{N}(t) \tag{5.4}$$

where $\mathcal{N}(t)$ is the summation of the signal-noise cross terms and the noise-noise term. It can be approximated as a Gaussian variable with zero mean. Defining $R_{ss}^{(b_m)} = \int_{-\infty}^{+\infty} s_{b_m}(t) s_{b_m}(t + \tau) dt$ and $R_{gg}(\tau) = \int_{-\infty}^{\infty} g(t) g(t + \tau) dt$, similar to the derivation in eq. (3.9) we have

$$\frac{E_b}{2N_f} \int_{t_b}^{t_e} q_{b_m}(t) q^*_{b_m}(t - T_d) dt = \frac{E_b}{2N_f} [R_{ss}^{(b_m)}(T_d) E_h + \sum_{l=0}^{K-1} \sum_{\substack{k=0 \\ k \neq l}}^{K-1} \alpha_l \alpha_k^* R_{ss}^{(b_m)}(|T_d - \tau_l + \tau_k|)] \tag{5.5}$$

where

$$R_{ss}^{(b_m)}(T_d) = b_m R_{gg}(0)(2N_f - 1). \tag{5.6}$$

Therefore,

$$\mathrm{E}[\mathrm{Re}\{D_m\}] = \frac{E_b}{2N_f}\{b_m(2N_f-1)E_hR_{gg}(0) + \mathrm{Re}[\sum_{l=0}^{K-1}\sum_{\substack{k=0\\k\neq l}}^{K-1}\alpha_l\alpha_k^* R_{ss}^{(b_m)}(|T_d-\tau_l+\tau_k|)]\}. \tag{5.7}$$

Defining

$$A = E_bE_hR_{gg}(0)(1-\frac{1}{2N_f})$$

and

$$B_{b_m} = \frac{E_b}{2N_f}\mathrm{Re}\big[\sum_{l=0}^{K-1}\sum_{\substack{k=0\\k\neq l}}^{K-1}\alpha_l\alpha_k^* R_{ss}^{(b_m)}(|T_d-\tau_l+\tau_k|)\big],$$

the expectation of the decision variable for transmitting data b_m in (5.7) is written as

$$m_D(b_m) = \mathrm{E}[\mathrm{Re}\{D_m\}] = b_mA + B_{b_m}. \tag{5.8}$$

Eq. (5.8) shows the expectation of the decision variable consists of two parts: the first term b_mA is in linear proportion to the transmitted data b_m; the second term B_{b_m} involves the data b_m, the pulse shape and the multipath channel and not necessarily has a clean linear relation with b_m., i.e., $B_{1+} \neq B_{-1}$. Due to this non-linear factor, the ultimate decision variable pair $m_D(+1)$ is not equal to $-m_D(-1)$, and the optimal threshold is non-zero. If we still apply 0 as the decision threshold following conventional bipolar systems, the bit resulting in larger $|m_D|$ will have less error rate than the other bit. For a given channel realization, either "+1" or "-1" will dominate the error occurrence. To ensure that two data bits would be 'treated' equally so that the same error probability will be obtained in the end, from the maximum likelihood

criterion, the optimal threshold leading to the minimum average BER is given by

$$\xi = \frac{1}{2}\left[m_D(+1) + m_D(-1)\right] = \frac{1}{2}\{A + B_{+1} - A + B_{-1}\} = \frac{1}{2}\{B_{+1} + B_{-1}\}. \quad (5.9)$$

Since B_{b_m} is a complicated term involving data, pulse shape and channel condition, the optimal threshold is channel dependent and therefore should be adaptively adjusted to the channel condition.

5.3 The Adaptive Threshold Scheme

In this section, a simple algorithm is developed to determine the optimal threshold for the TR pulse cluster system. Following (5.4), the optimal threshold is computed by

$$\xi_{optm} = \frac{1}{2}\left[m_D(+1) + m_D(-1)\right] = \frac{E_b}{4N_f}\int_{t_b}^{t_e} \mathrm{Re}\{q_{+1}(t)q_{+1}^*(t-T_d)dt + q_{-1}(t)q_{-1}^*(t-T_d)\}dt \quad (5.10)$$

Following exactly the same simplification methodology as in (4.13), the expression of ξ_{optm} can be simplified as

$$\begin{aligned} \xi_{optm} &= \frac{E_b}{4N_f}\int_{t_b}^{t_e} \mathrm{Re}\{q_{+1}(t)q_{+1}^*(t-T_d) + q_{-1}(t)q_{-1}^*(t-T_d)\}dt \\ &= \frac{E_b}{2N_f}\mathrm{Re}\{\int_{t_b}^{t_e} y(t)y^*(t-T_d)dt + \int_{t_b}^{t_e} y(t-T_d)y^*(t-2T_d)dt\}. \end{aligned} \quad (5.11)$$

The integration interval $[t_b, t_e]$ set is determined the same way as in Chapter 3, where $t_b = T_d + T_l$, $t_e = T_d + (2N_f - 1)T_d + T_h$, and $[T_l, T_h]$ as the beginning and end paths of the channel with magnitude larger than a fraction of the channel maximum magnitude. Depending on the channel model, the actual interval obtained by this

method can vary from hundreds of nanoseconds to microseconds, but always much larger then T_d. Therefore, we can use the approximation

$$\int_{t_b}^{t_e} y(t)y^*(t-T_d)dt = \int_{t_b+T_d}^{t_e+T_d} y(t-T_d)y^*(t-2T_d)dt \approx \int_{t_b}^{t_e} y(t-T_d)y^*(t-2T_d)dt \tag{5.12}$$

and eq. (5.11) can be reduced to

$$\xi_{optm} = \frac{E_b}{N_f}\mathrm{Re}\{\int_{t_b}^{t_e} y(t)y^*(t-T_d)\}dt \tag{5.13}$$

which only involves one signal structure $y(t)$. This has significantly reduced the complexity of the optimal threshold expression proposed in (5.10).

To calculate the value of (5.13) for a target channel, there are two options: 1) estimate $y(t)$ and then compute $\int y(t)y^*(t-T_d)dt$; 2) estimate $\int y(t)y^*(t-T_d)dt$ directly. The first method involves sending training symbols then averaging over the received waveforms to estimate $y(t)$. This operation requires either a high sampling rate for digital averaging or symbol long delay lines for analog averaging, and neither of them is desirable for practical implementation. Therefore the second method is chosen, i.e., to estimate $\int y(t)y^*(t-T_d)dt$ directly.

To estimate $\int y(t)y^*(t-T_d)dt$, a training sequence containing N half-TRPC pulses is sent over the multipath channel, with mathematical expression

$$f(t) = \sqrt{\frac{E_b}{2N_f}}\sum_{l=0}^{N-1}[x(t-lT_s)]. \tag{5.14}$$

The received signal is

$$r(t) = f(t) \otimes h(t) + n(t) = \sqrt{\frac{E_b}{2N_f}} \sum_{l=0}^{N-1} y(t - lT_s) + n(t). \tag{5.15}$$

Then an integration-and-dump (I&D) device is used to obtain the decision variable D_m for the m-th training bit. Assuming timing has been acquired for t_b and t_e, we have

$$D_m = \int_{mT_s+t_b}^{mT_s+t_e} r(t) r^*(t - T_d) dt. \tag{5.16}$$

The estimated threshold is obtained by

$$\hat{\xi} = \mathrm{Re}\{\frac{2}{N} \sum_{m=0}^{N-1} D_m\}. \tag{5.17}$$

From (5.16), we have

$$\begin{aligned} D_m &= \int_{mT_s+t_b}^{mT_s+t_e} \{\sqrt{\frac{E_b}{2N_f}} \sum_{l=0}^{N-1} y(t - lT_s) + n(t)\}\{\sqrt{\frac{E_b}{2N_f}} \sum_{l=0}^{N-1} y^*(t - lT_s - T_d) + n^*(t - T_d)\} dt \\ &= \int_{t_b}^{t_e} \{\sqrt{\frac{E_b}{2N_f}} y(t) + n(t + mT_s)\}\{\sqrt{\frac{E_b}{2N_f}} y^*(t - T_d) + n^*(t + mT_s - T_d)\} dt \\ &= \frac{E_b}{2N_f} \int_{t_b}^{t_e} y(t) y^*(t - T_d) dt + \mathcal{N}_m(t) \end{aligned} \tag{5.18}$$

where $\mathcal{N}_m(t)$ $(m = 0, 1, ..., N-1)$ all have approximately zero mean. The estimation given by (5.17) is unbiased since from (5.18), we have

$$\mathrm{E}[\mathrm{Re}\{\frac{2}{N} \sum_{m=0}^{N-1} D_m\}] = \mathrm{Re}\{\frac{E_b}{N_f} \int_{t_b}^{t_e} y(t) y^*(t - T_d) dt\} = \xi_{optm}. \tag{5.19}$$

Since the optimal threshold is channel dependent, such a training and threshold estimation procedure should be performed regularly to track the changes in channel condition so that the threshold adapts to different channels.

5.4 Simulation Results and Discussion

In this section, we present simulation results for the performance of the adaptive threshold scheme in the TR pulse cluster structure. The system setup is the same as that of Chapter 3. The channel models chosen for simulation are IEEE 802.15.4a CM1-CM8 channels. CM1 and CM2 model the residential line-of-sight (LOS) and non-line-of-sight (NLOS) channels, CM3 and CM4 model the office LOS and NLOS channels, CM5 and CM6 model the outdoor LOS and NLOS channels, CM7 and CM8 model the industrial LOS and NLOS channels [21]. In the simulation, t_b and t_e are determined by the method described in Section 5.3. For each channel model, the final BER is obtained by averaging the BERs of 100 channel realizations. In all the figures, the solid lines represent the proposed adaptive scheme using the "estimated threshold" obtained from (5.17), and the dashed lines represent the "old threshold" 0.

Fig. 5.1 shows the BER performance in residential environments. In CM1 channels, at BER $= 10^{-4}$, the adaptive threshold outperforms the "old threshold" by about 1.6 dB. In CM2 channels, to achieve BER$= 10^{-4}$, the new scheme saves 2.0 dB compared to the old threshold scheme. Fig. 5.2 presents that at BER$= 2.0 \times 10^{-4}$, around 2.0 dB power is saved by applying the estimated adaptive threshold in both CM3 and CM4 channels. Fig. 5.3 shows the BER performance in outdoor environments. Performance gains of over 1.6 dB and 0.5 dB are achieved at BER$=10^{-4}$

in CM5 and CM6 channels, respectively. Fig. 5.4 shows that at BER = 10^{-4} in CM7 and CM8 channels, adaptive threshold outperforms the fixed threshold 0 by about 3.2 dB and 0.8 dB respectively. In general channels with more severe IPI and hence asymmetry for bit "+1" and "-1" benefit more substantially from the adaptive threshold scheme.

Fig. 5.5 shows that at BER = 2.0×10^{-4} in CM1 channels, the adaptive threshold scheme obtained from (5.17) using different training lengths outperforms the old threshold scheme by 1.1 to 1.5 dB. The performance using ideal threshold computed by (5.10) is also given for comparison. By increasing the length of the training sequence from 5 to 15, the performance is improved accordingly. The gain obtained from using a training sequence longer than 15 is small since the performance of N=15 is already very close to that of the ideal threshold. Comparing Fig. 5.1 and Fig. 5.5, $N = 30$ leads to the identical performance to the "ideal threshold".

5.5 Conclusion

In this chapter, a simple adaptive threshold algorithm designed for the TR pulse cluster system has been proposed. In the previous TR pulse cluster system, the conditional bit error rates of "+1" and "-1" are distinct and normally one is much larger than the other. By adopting the adaptive threshold in the detection, the larger BER for one bit is reduced greatly while the smaller BER for other bit is only slightly increased. Consequently, the overall performance is largely improved by introducing this adaptive threshold. Simulation results have shown that the new scheme achieves more power savings for channels that have strong asymmetry for "+1" and "-1".

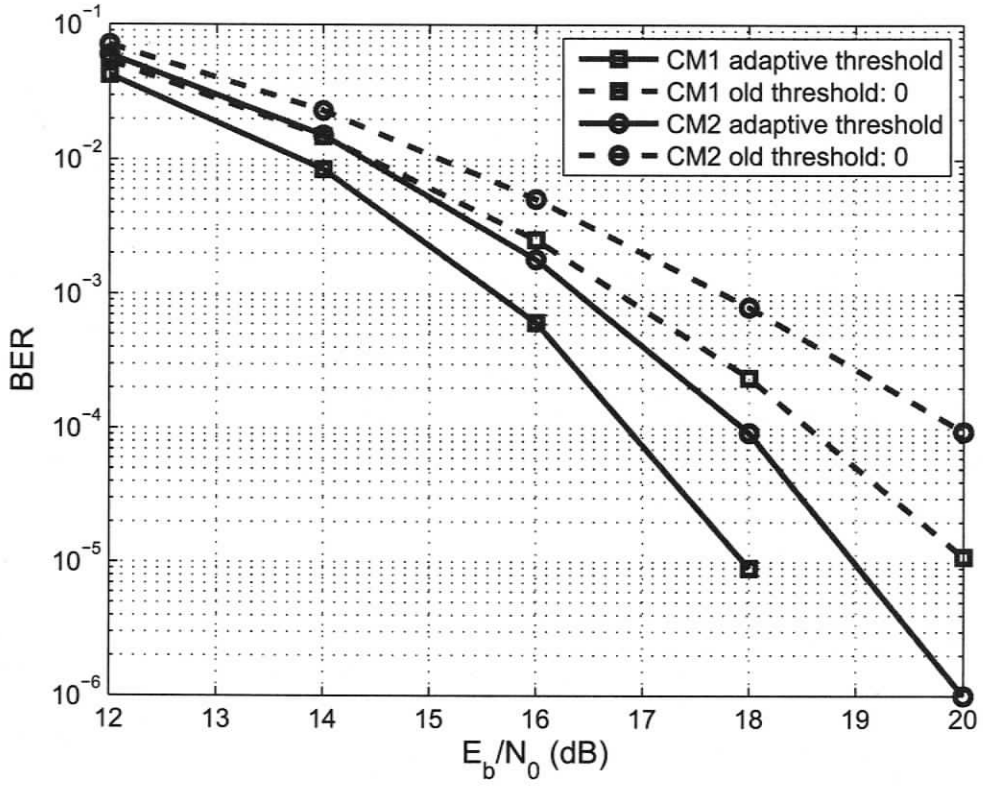

Figure 5.1: The BER of the TR pulse cluster in residential environments using the new adaptive threshold method (N=30).

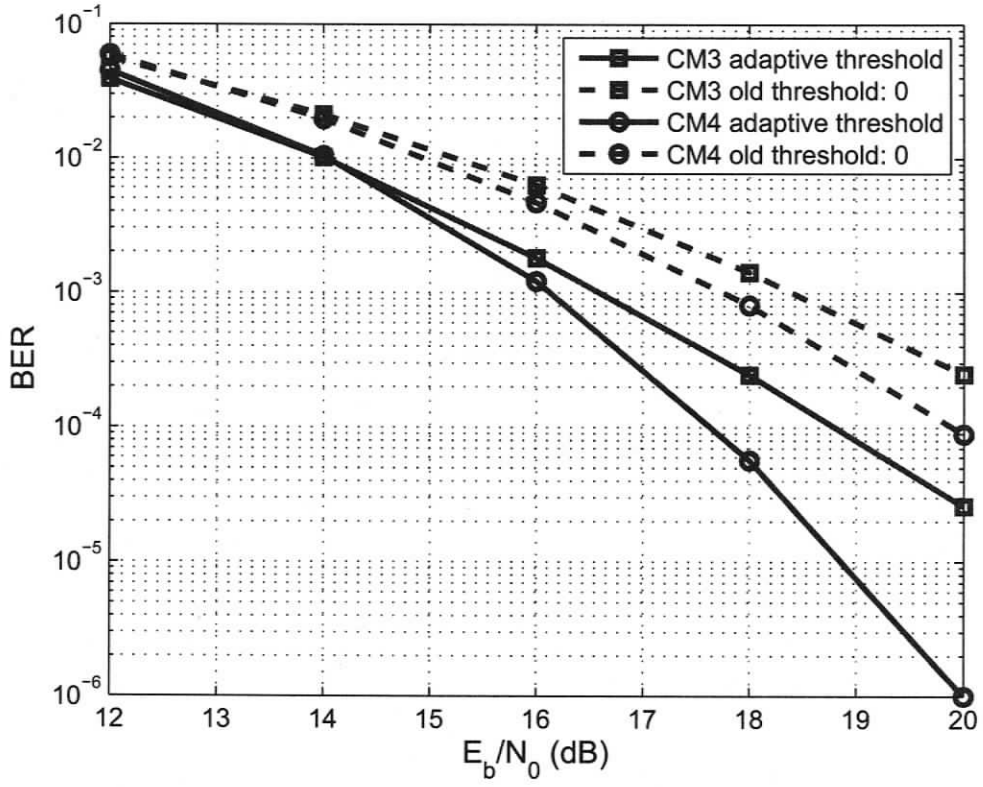

Figure 5.2: The BER of the TR pulse cluster in office environments using the new adaptive threshold method (N=30).

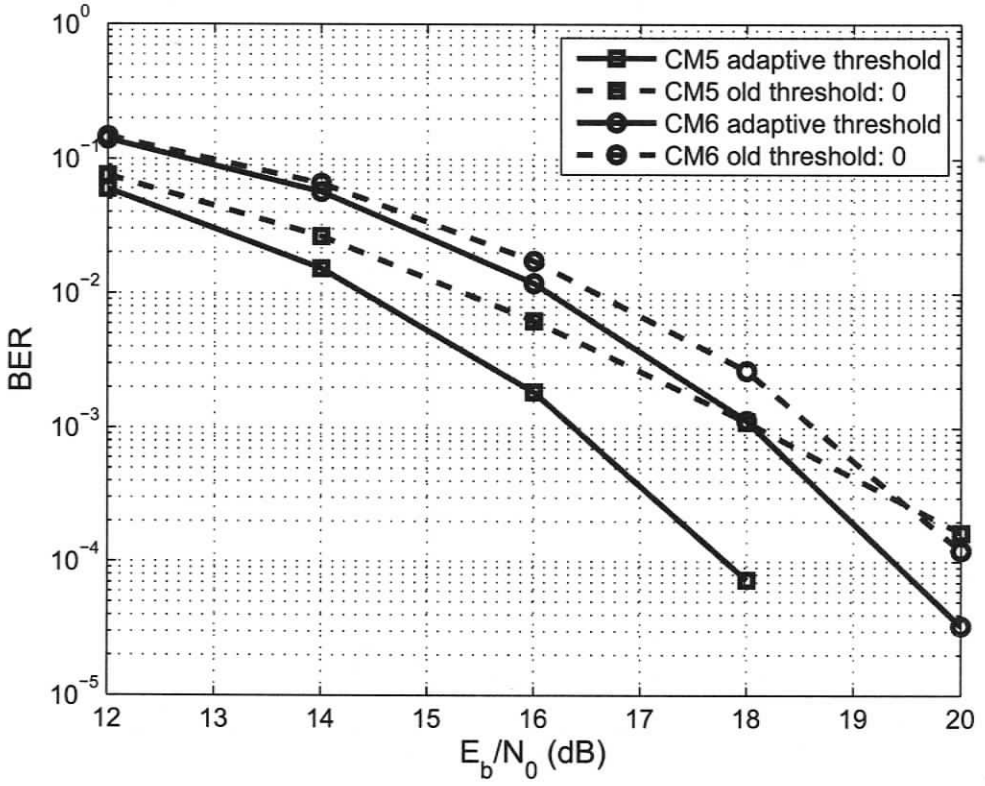

Figure 5.3: The BER of the TR pulse cluster in outdoor environments using the new adaptive threshold method (N=30).

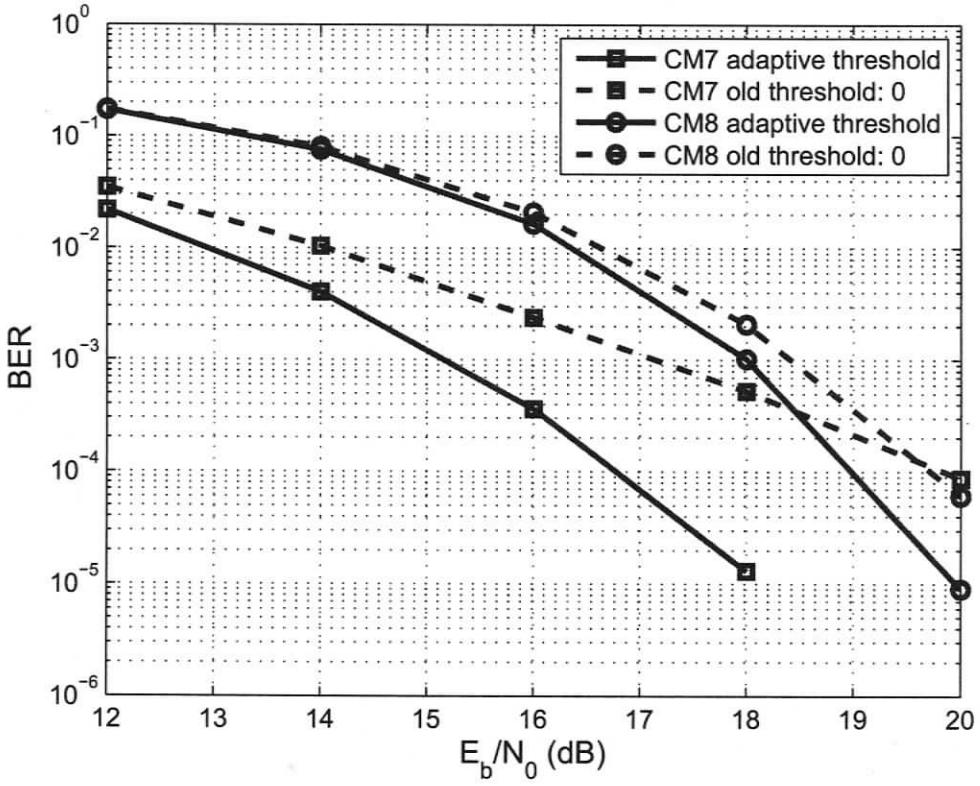

Figure 5.4: The BER of the TR pulse cluster in industrial environments using the new adaptive threshold method (N=30).

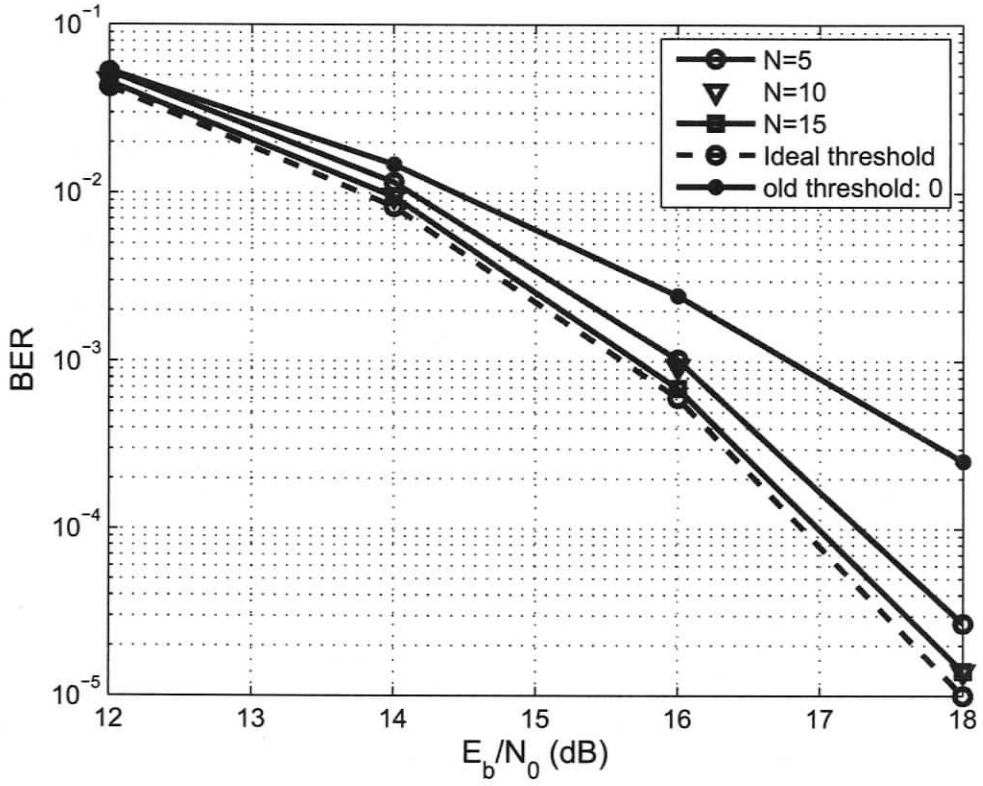

Figure 5.5: The BER of the TR pulse cluster in CM1 using estimated threshold with different training lengths.

Chapter 6

Conclusion and Future Work

6.1 Conclusions

Ultra-wideband is a fast burgeoning technology with inviting features in wireless communications. Compared to narrow-band technologies, UWB has greater channel resolution capacity thanks to its extremely narrow pulses. While the same time as those pulses make the accurate localization possible in the UWB world, they also pose a tremendous challenge on the receiver design, particularly on the channel estimation. Although the transmitted reference technique overcomes the tedious channel estimation by using reference pulses, the required long analog delay lines make the implementation difficult and costly. In this thesis a novel transmitting pattern named transmitted reference pulse cluster has been proposed for low data rate UWB communication, which allows a simple and robust receiver to be implemented, with symbol rate sampling and short delay lines.

Unlike conventional TR systems that use pulse pairs, the TRPC structure transmits a cluster of evenly spaced pulses. The pulses at even positions must have the same polarity, so do the pulses at the odd positions. The relative polarity between

even and odd positions carries information. This makes TRPC unique because all the pulses are closely packed and evenly distributed. The closely positioned pulse pairs means shorter analog delay lines at the receiver end and makes the implementation easier. The evenly distributed pulse clusters, with the delay-and-multiply detection mechanism, successfully compensate the 3 dB loss from the reference pulses and helps TRPC achieve superior performance over existing techniques, including non-coherent PPM with energy detection, conventional TR, and frequency shifted reference systems in multipath UWB channels.

The integration interval determination for the TRPC system has been studied in Chapter 4. Three new practically implementable algorithms have been proposed. Among them, the threshold-crossing method has the lowest complexity but inferior performance, and requires a long training length and relatively high sampling rate. The BER minimization based method has the best BER performance and the lowest requirement on sampling rate and training length but requires a two-dimensional search for the optimal interval. The hybrid method yielded similar performance to the BER minimization based method in most cases, with much reduced complexity.

By nature, TRPC is not inter-pulse interference free because of the closely placed pulses. Apart from limited performance drop because of that, the TRPC also exhibits a uniquely unbalanced conditional bit error rate, i. e., the error rate of "+1" and "-1" are distinct and normally one is much larger than the other. In Chapter 5, an adaptive threshold methodology has been introduced. Instead of using absolute zero as the detection threshold, an adaptive threshold is applied, which greatly decreases the BER for one bit and only slightly increases the BER for the other bit. Consequently, the overall performance is significantly improved, and can achieve more power savings

for channels that have strong asymmetry for "+1" and "-1".

6.2 Future Work

The system model of TRPC system and a series of methodologies are proposed for its performance optimization.

1. The work of this thesis is based on single user case. In real systems, multiple users can exist simultaneously to share the same bandwidth and inevitably interfere with each other. The TRPC communication system with multiple access in both up-streaming and downstreaming transmission becomes an interesting topic. The most straightforward approach for multiple-user TRPC is time division multiple access.

2. Chapter 5 is based on the regular threshold-crossing technique and Chapter 4 used absolute zero as the detection threshold. If the receiver can apply the adaptive threshold to the optimal integration interval, the system performance can be further improved. Further study could focus on combining the two techniques in the TRPC system.

Bibliography

[1] *Ultra-Wideband Opportunities Under the New FCC Waiver.* Freescale Semiconductor, Mar. 2005.

[2] J. Reed, *An Introduction to Ultra Wideband Communication Systems.* Prentice Hall PTR, 2005.

[3] L. Yang and G. B. Giannakis, "Ultra-wideband communications: An idea whose time has come," pp. 27–54, Nov. 2004.

[4] R. Hoctor and H. Tomlinson, "Delay-hopped transmitted-reference RF communications," " in *IEEE Conf. Ultra Wideband Syst. Techno.*, pp. 265–269, May 2002.

[5] T. Q. S. Quek and M. Win, "Analysis of UWB transmitted-reference communication systems in dense multipath channels," pp. 1863–1874, Sep. 2005.

[6] N. V. Stralen, A. Dentinger, K. W. II, R. Hoctor, and H. Tomlinson, "Delay-hopped transmitted-reference experimental results," " in *IEEE Conf. Ultra Wideband Syst. Techno.*, pp. 93–98, May 2002.

[7] H. Zhang and D. L. Goeckel, "Generalized transmitted-reference UWB systems," " in *IEEE Conf. Ultra Wideband Syst. Techno.*, pp. 16–19, Nov. 2003.

[8] S. Franz and U. Mitra, "On optimal data detection for UWB transmitted reference systems," " in *Globecom*, pp. 744–748, Dec. 2003.

[9] Y.-L. Chao and R. A. Scholtz, "Optimal and suboptimal receivers for ultra-wideband transmitted reference systems," " in *Globecom*, pp. 759–763, Dec. 2003.

[10] J. D. Choi and W. E. Stark, "Performance of ultra-wideband communications with suboptimal receivers in multipath channels," pp. 1754–1766, Dec. 2002.

[11] S. Gezici, F. Tufvesson, and A. F. Molisch, "On the performance of transmitted-reference impulse radio," " in *Globecom*, pp. 2874–2879, Nov. 2004.

[12] K. Witrisal, G. Leus, M. Pausini, and C. Krall, "Equivalent system model and equalization of differential impulse radio UWB," pp. 1851–1862, Sep. 2005.

[13] Y.-L. Chao and R. A. Scholtz, "Ultra-wideband transmitted reference systems," pp. 1556–1569, Sep. 2005.

[14] Z. Xu, B. M. Sadler, and J. Tang, "Data detection for UWB transmitted reference systems with inter-pulse interference," in *ICASSP*, vol. III, pp. 601–604, 2005.

[15] W. Gifford and M. Win, "On transmitted-reference UWB communications," " in *Proc. Asilomar Conf. Signals, Systems and Computers*, pp. 1526–1531, Nov. 2004.

[16] M. Casu and G. Durisi, "Implementation aspects of a transmitted-reference UWB receiver," *Wireless Communications and Mobile Computing*, pp. 537–549, Aug. 2005.

[17] D. L. Goeckel and Q. Zhang, "Slightly frequency-shifted reference ultra-wideband (uwb) radio," *IEEE Trans. Commun.*, pp. 508–519, Mar. 2007.

[18] X. Dong, A. C. Y. Lee, and L. Xiao, "A new UWB dual pulse transmission and detection technique," " in *ICC*, pp. 2835–2839, May 2005.

[19] X. Dong, L. Xiao, and A. C. Y. Lee, "Performance analysis of dual pulse transmission in UWB channels," *IEEE Commun. Lett.*, Aug. 2006.

[20] Q. H. Dang, A. Trindade, A.-J. van der Veen, and G. Leus, "Signal model and receiver algorithms for a transmit-reference ultra-wideband communication system," *IEEE J. Select. Areas Commun.*, pp. 773–779, Apr. 2006.

[21] A. F. Molisch, K. Balakrishnan, C.-C. Chong, S. Emami, A. Fort, J. Karedal, J. Kunisch, H. Schantz, U. Schuster, and K. Siwiak, "IEEE 802.15.4a channel model - final report," " in *IEEE P802.15-04-0662-00-004a*, Oct. 2004.

[22] A. A. M. Saleh and R. A. Valenzuela, "A statistical model for indoor multpath progagation," vol. 5, no. 2, pp. 128–137, Feb. 1987.

[23] I. Lakkis, "Modulation summary for tg4a," IEEE P802.15-05-617-01-004a, Tech. Rep., Oct. 2005.

[24] F. Tufvesson and A. F. Molisch, "Ultra-wideband communication using hybrid matched filter correlation receivers," " in *IEEE Conf. Vehicular Techno.*, pp. 1290 – 1294, May 2004.

[25] F. Tufvesson, S. Gezici, and A. F. Molisch, "Ultra-wideband communications using hybrid matched filter correlation receivers," vol. 5, pp. 3119–3129, Nov. 2006.

[26] S. Franz and U. Mitra, "Integration interval optimization and performance analysis for uwb transmitted reference systems," " in *UWBST&IWUWBS*, pp. 26 – 30, May 2004.

[27] G. Leus and A.-J. van der Veen, "A weighted autocorrelation receiver for transmitted reference ultra wideband communications," " in *Signal Processing Advances in Wireless Communications, 2005 IEEE 6th Workshop on*, pp. 965–969, Jun. 2005.

[28] R. Zhang and X. Dong, "Synchronization and integration region optimization for UWB TR signals," " in *IEEE Wireless Commun. Networking Conf., 2007*, pp. 1577–1582, Mar. 2007.

[29] X. Dong, L. Jin, and P. Orlik, "A new transmitted reference pulse cluster system for UWB communications," to appear. [Online]. Available: http://www.ece.uvic.ca/~xdong/VT2007-00108.pdf

[30] S. He, X. Dong, Z. Tian, T.-K. Liu, M. Ghoreishi, M. McGuire, S. Neville, and N. Tin, "On the empirical evaluation of spatial and temporal characteristics of ultra-wideband channel," " in *Vehicular Technology Conference*, pp. 1–5, 2009.

Appendix A

Derivation of noise-noise product in eq.(4.5)

In this appendix, we derive the approximation arrived for the variance of the noise-noise product term in the decision variable in eq.(4.5).

$$\begin{aligned}\sigma_4^2(t_b,t_e) &= \frac{1}{2}\mathrm{E}\{\int_{t_b}^{t_e}\int_{t_b}^{t_e} n(t)n^*(t-T_d)n^*(u)n(u-T_d)dtdu\} \\ &= \frac{1}{2}\int_{t_b}^{t_e}\int_{t_b}^{t_e}\mathrm{E}\{n(t)n^*(t-T_d)n^*(u)n(u-T_d)\}dtdu \qquad \text{(A.1)}\end{aligned}$$

As the noise random process is complex Gaussian, and recalling from the previous definition $R_n(\tau) = \mathrm{E}\{n^*(u)n(u+\tau)\} = N_0 R_{tr}(\tau)$, we have

$$\begin{aligned}&\mathrm{E}\{n(t)n^*(t-T_d)n^*(u)n(u-T_d)\} \\ =\ &\mathrm{E}\{n(t)n^*(t-T_d)\}\mathrm{E}\{n^*(u)n(u-T_d)\} + \mathrm{E}\{n(t)n^*(u)\}\mathrm{E}\{n^*(t-T_d)n(u-T_d)\} \\ &+\mathrm{E}\{n(t)n(u-T_d)\}\mathrm{E}\{n^*(t-T_d)n^*(u)\} \\ =\ &N_0^2 R_{tr}(T_d)T_{tr}(-T_d) + N_0^2 R_{tr}(t-u)T_{tr}(u-t) \approx N_0^2 R_{tr}^2(t-u) \qquad \text{(A.2)}\end{aligned}$$

As mathematically $R_{tr}(\tau) = B\text{sinc}(B\tau)$, we can see when B assumes a large value, $R_{tr}(\tau)$ becomes more peaky and thus has a very small non-zero support region, i.e., $R_{tr}(\tau) = B\text{sinc}(B\tau) \approx 0$ when $|\tau| > T_p$. Therefore, combining eq. (A.1) and (A.2), there is

$$\begin{aligned}\sigma_4^2(t_b, t_e) &= \frac{1}{2}\int_{t_b}^{t_e}\int_{t_b}^{t_e} N_0^2 R_{tr}^2(t-u)dtdu \approx \frac{N_0^2}{2}\int_{t_b}^{t_e}\int_{u-T_p}^{u+T_p} R_{tr}^2(t-u)dtdu \\ &\approx \frac{N_0^2}{2}\int_{t_b}^{t_e}\int_{-T_p}^{T_p} R_{tr}(\tau)^2 d\tau du = \frac{N_0^2}{2}(t_e - t_b)\int_{-T_p}^{T_p} R_{tr}(\tau)^2 d\tau \qquad \text{(A.3)}\end{aligned}$$

Appendix B

Derivation of signal-noise product in eq.(4.6)

In this appendix, we derive the approximation arrived for the variance of the noise-noise product term in the decision variable in eq.(4.6).

For notational brevity, we use $q(t)$, b, $\sigma_{23}^2(b)$ to replace $q_{b_m}(t)$, b_m, $\sigma_{23}^2(t_b, t_e|b_m)$ respectively in this appendix. Since $R_{tr}(\tau) = B\text{sinc}(B\tau)$, where $B/2$ is the bandwidth of the transmitted UWB pulse cluster, we have

$$\begin{aligned}
&\int_{t_b}^{t_e}\int_{t_b}^{t_e} q(t)q^*(t')R_{tr}(t'-t)dtdt' = \int_{t_b}^{t_e}\int_{t_b}^{t_e} q^*(t')q(t)B\text{sinc}(B(t'-t))dtdt' \\
= &\int_{t_b}^{t_e}\int_{t_b}^{t_e} q^*(t')q(t)\frac{e^{j\pi B(t'-t)} - e^{-j\pi B(t'-t)}}{2j\pi(t'-t)}dtdt' = \int_{t_b}^{t_e}\int_{t_b}^{t_e} q^*(t')q(t)\int_{-B/2}^{B/2} e^{j2\pi f(t'-t)}dfdtdt' \\
= &\int_{t_b}^{t_e} q^*(t')\int_{-B/2}^{B/2}\int_{t_b}^{t_e} q(t)e^{j2\pi f(t'-t)}dtdfdt' \approx \int_{t_b}^{t_e} q^*(t')\int_{-B/2}^{B/2} Q(f)e^{j2\pi ft'}dfdt' \\
= &\int_{t_b}^{t_e} q^*(t')q(t')dt' = \int_{t_b}^{t_e} |q^2(t)|dt \qquad \text{(B.1)}
\end{aligned}$$

where $Q(f) = \int_{-\infty}^{\infty} q(t)e^{-j2\pi ft}dt$. The approximation in (B.1) is justified as the inter-

val $[t_b, t_e]$ covers the majority of the channel energy. Applying similar approximation, $\sigma_{23}^2(b)$ in (4.4) is approximated as

$$\sigma_{23}^2(b) \approx \frac{E_b N_0}{4N_f} \int_{t_b}^{t_e} |q^2(t)|dt + \frac{E_b N_0}{4N_f} \int_{t_b}^{t_e} |q^2(t-T_d)|dt + \frac{E_b N_0}{2N_f} \int_{t_b}^{t_e} \mathrm{Re}\{q^*(t)q(t-2T_d)\}dt \tag{B.2}$$

where $q(t)$ can be expressed as

$$\begin{aligned} q(t) &= \sum_{k=0}^{K-1} \sum_{i=0}^{N_f-1} \alpha_k [g_r(t-\tau_k-2iT_d) + b \cdot g_r(t-\tau_k-2iT_d-T_d)] \\ &= y(t) + b \cdot y(t-T_d). \end{aligned} \tag{B.3}$$

Since T_d is very small compared to the integration length $(t_e - t_b)$ and the integration interval $[t_b, t_e]$ covers the majority of the channel energy, we can use the following three approximations: $\int_{t_b}^{t_e} |q(t)|^2 dt \approx \int_{t_b}^{t_e} |q(t-T_d)|^2 dt$, $\int_{t_b}^{t_e} |y(t)|^2 dt \approx \int_{t_b}^{t_e} |y(t-T_d)|^2 dt$, and $\int_{t_b}^{t_e} \mathrm{Re}\{y(t) \cdot y^*(t-2T_d)\}dt \approx \int_{t_b}^{t_e} \mathrm{Re}\{y(t-T_d) \cdot y^*(t-3T_d)\}dt$. Moreover, we have

$$\begin{aligned} y(t) \cdot y^*(t-2T_d) &= \sum_{k=0}^{K-1} \sum_{i=0}^{N_f-1} \alpha_k g_r(t-\tau_k-2iT_d) \sum_{l=0}^{K-1} \sum_{j=0}^{N_f-1} \alpha_l^* g_r(t-\tau_l-2(j+1)T_d) \\ = & \left[\sum_{k=0}^{K-1} \sum_{i=1}^{N_f-1} \alpha_k g_r(t-\tau_k-2iT_d) + \sum_{k=0}^{K-1} \alpha_k g_r(t-\tau_k) \right] \\ \cdot & \left[\sum_{l=0}^{K-1} \sum_{j=0}^{N_f-2} \alpha_l^* g_r(t-\tau_l-2(j+1)T_d) + \sum_{k=0}^{K-1} \alpha_l^* g_r(t-\tau_l-2N_fT_d) \right] \\ = & \left| \sum_{k=0}^{K-1} \sum_{i=1}^{N_f-1} \alpha_k g_r(t-\tau_k-2iT_d) \right|^2 + \eta \end{aligned} \tag{B.4}$$

where $|\mathrm{Re}\{\eta\}| < |\sum_{k=0}^{K-1} \sum_{i=1}^{N_f-1} \alpha_k g_r(t-\tau_k-2iT_d)|^2$ is awalys satisfied. Therefore, $\mathrm{Re}\{y(t) \cdot y^*(t-2T_d)\} \geq 0$. Since the major part of the UWB pulse $g_r(t)$ is limited

in the T_d-width range, it is obvious that $x(t-2iT_d)$ and $x(t-(2j+1)T_d)$ are quasi-orthogonal pairs for $i,j=0,1,2,\cdots$. Therefore, $\mathrm{Re}\{\int_{t_b}^{t_e} y^*(t-2iT_d)y(t-(2j+1)T_d)dt\}$ should be small and approximately equal for different i and j's. Hence, there is $\int_{t_b}^{t_e}\mathrm{Re}\{y^*(t-T_d)y(t-2T_d)\}dt \approx \int_{t_b}^{t_e}\mathrm{Re}\{y^*(t)y(t-3T_d)\}dt$.

Based on the above discussions, (B.2) can be further approximated as

$$\sigma_{23}^2(b) \approx \frac{E_bN_0}{2N_f}\Big[\int_{t_b}^{t_e}|q(t)|^2dt + \int_{t_b}^{t_e}\mathrm{Re}\{q^*(t)q(t-2T_d)\}\Big]dt \tag{B.5}$$

where

$$\begin{aligned}
&\int_{t_b}^{t_e}|q(t)|^2dt = \int_{t_b}^{t_e} q(t)\cdot q^*(t)dt \\
=\ &\int_{t_b}^{t_e}[y(t)+b\cdot y(t-T_d)]\cdot[y^*(t)+b\cdot y^*(t-T_d)]dt \\
=\ &\int_{t_b}^{t_e}[|y(t)|^2+|y(t-T_d)|^2]dt + b\cdot 2\cdot \underbrace{\int_{t_b}^{t_e}\mathrm{Re}\{y(t)\cdot y^*(t-T_d)\}dt}_{\triangleq\xi_1} \\
\approx\ &2\int_{t_b}^{t_e}|y(t)|^2dt + 2b\xi_1,
\end{aligned} \tag{B.6}$$

and

$$\begin{aligned}
& \int_{t_b}^{t_e} \mathrm{Re}\{q^*(t)q(t-2T_d)\}dt \\
= & \int_{t_b}^{t_e} \mathrm{Re}\{[y^*(t)+b\cdot y^*(t-T_d)]\cdot[y(t-2T_d)+b\cdot y(t-3T_d)]\}dt \\
= & \int_{t_b}^{t_e} \mathrm{Re}\{y^*(t)y(t-2T_d)+y^*(t-T_d)y(t-3T_d)\}dt \\
+ & \; b\int_{t_b}^{t_e} \mathrm{Re}\{y^*(t-T_d)y(t-2T_d)+y^*(t)y(t-3T_d)\}dt \\
\approx & \; 2\int_{t_b}^{t_e} \mathrm{Re}\{y^*(t)y(t-2T_d)\}dt + 2b\underbrace{\int_{t_b}^{t_e} \mathrm{Re}\{y^*(t-T_d)y(t-2T_d)\}dt}_{\triangleq\xi_2} \\
= & \; 2\int_{t_b}^{t_e} \mathrm{Re}\{y^*(t)y(t-2T_d)\}dt + 2b\xi_2. \qquad \text{(B.7)}
\end{aligned}$$

In addition,

$$\begin{aligned}
& \Big|\int_{t_b}^{t_e} \mathrm{Re}\{q(t)q^*(t-T_d)\}dt\Big| \\
= & \Big|\int_{t_b}^{t_e} \mathrm{Re}\{[y(t)+b\cdot y(t-T_d)]\cdot[y^*(t-T_d)+b\cdot y^*(t-2T_d)]\}dt\Big| \\
= & \Big|\underbrace{\int_{t_b}^{t_e} \mathrm{Re}\{y(t)y^*(t-T_d)+y(t-T_d)y^*(t-2T_d)\}dt}_{=\xi_1+\xi_2} \\
+ & \; b\cdot\int_{t_b}^{t_e} \{|y(t-T_d)|^2+\mathrm{Re}\{y^*(t)y(t-2T_d)\}\}dt\Big| \\
= & \int_{t_b}^{t_e} |y(t-T_d)|^2dt + \int_{t_b}^{t_e} \mathrm{Re}\{y^*(t)y(t-2T_d)\}dt + b(\xi_1+\xi_2) \\
\approx & \int_{t_b}^{t_e} |y(t)|^2dt + \int_{t_b}^{t_e} \mathrm{Re}\{y^*(t)y(t-2T_d)\}dt + b(\xi_1+\xi_2). \qquad \text{(B.8)}
\end{aligned}$$

According to (B.6)-(B.8), we have

$$\int_{t_b}^{t_e} |q(t)|^2 dt + \int_{t_b}^{t_e} \mathrm{Re}\{q^*(t)q(t-2T_d)\}dt \approx 2\Big|\int_{t_b}^{t_e} \mathrm{Re}\{q(t)q^*(t-T_d)\}dt\Big|. \quad \text{(B.9)}$$

Finally, (B.5) can be approximated as

$$\begin{aligned} \sigma_{23}^2(b) &\approx \frac{E_b N_0}{2N_f}\Big[\int_{t_b}^{t_e} |q(t)|^2 dt + \int_{t_b}^{t_e} \mathrm{Re}\{q^*(t)q(t-2T_d)\}\Big]dt \\ &\approx \frac{E_b N_0}{2N_f}\cdot 2\Big|\int_{t_b}^{t_e} \mathrm{Re}\{q(t)q^*(t-T_d)\}dt\Big| = 2N_0\cdot\frac{E_b}{2N_f}\Big|\int_{t_b}^{t_e} \mathrm{Re}\{q(t)q^*(t-T_d)\}dt\Big| \\ &= 2N_0\mu(t_b,t_e|b_m). \end{aligned} \quad \text{(B.10)}$$

Acknowledgment

I would like to thank Dr. Zhonghua Liang for part of the mathematical derivations in this appendix.